UNIVERSITY OF CALIFORNIA, IRVINE

Advancing the Bijel Chemical Library: Expanding the Spectrum of Functional Materials

THESIS

Submitted in partial satisfaction of the requirements for the degree of

MASTER OF SCIENCE

In Chemical and Biomolecular Engineering

By

Bilal Ghassan Saudi

Thesis Committee:

Professor Ali Mohraz, Chair

Professor Elliot Botvinick, co-Chair

Professor Herdeline Ardoña

2023

Dedication

To

my mother

for putting me through graduate school while showing countless love and support

and

my father

for his encouragement, wise guidance, and unconditional support

TABLE OF CONTENTS

LIST OF FIGURES

LIST OF TABLES

ACKNOWLEDGEMENTS

Thank you, Ali, for welcoming me into the lab during my undergraduate years and continuing to guide me throughout my graduate studies. Your teaching and mentorship have played a crucial role in shaping my growth as an engineer and allowed me to spark a profound interest in this field.

Thank you, Elliot, for being one of the most optimistic and compassionate professors at UCI. Your continuous recognition of my work allowed me to be my best through challenging moments, pushing me to succeed. Our memorable kayaking adventures, Eureka dinners, and Friday lab meeting discussions and bagels are moments I will always cherish.

I extend my deepest gratitude to Luciano for his mentorship and guidance, which have shaped me into the best student and engineer I could be. From all of our white board discussions, BTM meetings, Downtown Disney milkshakes, and happy hour moments, thank you for being the person I could lean on for support.

To my SMEL and BEAMS lab-mates thank you for listening and providing feedback during our project discussions, giving assistance whenever needed, and being there to crack jokes with.

To my CBE friends in my cohort, thank you all for the late study sessions in the towers, countless memories laughing with each other, and allowing me to show you all around Irvine. You are the best group of people, and I can’t wait for you all to succeed.

To Cliff, thank you for taking me on your adventurous hiking journeys, showing me around the east coast, and being my best friend in graduate school.

Thank you to my parents, brother, sister, and childhood friends. For the countless support, encouragement, and love given to me during my time in college.

ABSTRACT OF THE THESIS

Advancing the Bijel Chemical Library: Expanding the Spectrum of Functional Materials

By

Bilal Ghassan Saudi
Master of Science in Chemical and Biomolecular Engineering
University of California, Irvine, 2023
Associate Professor, Ali Mohraz, Chair
Associate Professor, Elliot Botvinick, co-Chair

This thesis presents an engineered approach to create bicontinuous interfacially jammed emulsion gels (bijels), achieved through the kinetic arrest of temperature-induced spinodal decomposition within partially miscible binary fluids. The subsequent incorporation of these spinodal structures into 3D porous polymers forms the basis of bijel templated materials (BTMs), which offer distinct advantages over traditional porous materials. These advantages encompass tunable domain size, enhanced structural integrity, continuous morphology, and deformability. Initial methods to solidify bicontinuous architectures into interpenetrating porous scaffolds faced limitations in selecting suitable polymers, creating different geometries, and elongated processing times. To address these challenges, a new technique called intrinsically polymerizable bijels (IPBs) was developed, where one of the bicontinuous phases is a monomer. The aim of this research is to create a degradable BTM, serving as a bicontinuous mold, allowing for filling the void space with a polymerizable material followed by matrix degradation. Successful synthesis of disulfide diacrylate was achieved high yields

where partial miscibility of 1,2-pentanediol was found to have a transition temperature below room temperature. By experimentally determining the coexistence curve based on fluids miscibility, both the critical mass fraction and critical transition temperature were identified. Neutrally wetting nanoparticles were synthesized, and their surface was functionalized with various silanizing agents to optimize consistent results for proper bijel formation. Fine-tuning of polymerization and quenching conditions led to the production of a degradable porous BTM sheet. This process introduces a bijel templated invertible mold (BTIM) to expand the spectrum of functional materials with spinodal microstructures, with potential applications as porous coatings to enhance material and surface functionalization and interactions with its biological interface.

Chapter 1: Background

1.1 Motivation

Across the universe of science and engineering topics, porous materials find extensive applications in many fields including tissue engineering[1], catalysis[2], batteries[3], fuel cells[4,5], filtration devices[6], and environmental remediation[7]. These structures comprise two parts, a solid matrix or frame and a second void or pore phase, which can vary in size, distribution, and shape, each providing unique properties that optimize utilization in specific applications.[8] These properties have been shown to be critical in mitigating the foreign body response to different implantable biomaterials.[9–11] Additionally, pore size and microstructural morphology are being investigated to improve fluid permeability in controlled release systems and catalytic reactions.[12] Along with the advantages, there are limitations and drawbacks that can become challenging when incorporating these structures. For example, a key concern inherent to replacing solid material with void space is structural stability, strength, and durability, especially with repeated cycles stresses.[9,10] Moreover, natural porous materials also possess randomly sized domains, resulting in uncontrollable flow through their pores.[15,16]

One solution that could enhance many of the desired properties while simultaneously reducing the impact of the downfalls is bijel templated materials (BTMs). Bicontinuous interfacially jammed emulsion gels (bijels), the basis of BTMs, offer a novel category of porous materials characterized by a fully interpenetrating, continuous domain pathway comprising a uniform negative Gaussian curvature. BTMs offer a solution to the challenges commonly found in conventional porous materials by virtue of their tunable domain size and continuous morphology. To address issues like structural stability, BTMs incorporate interconnected channels, thereby enhancing mechanical

strength. As a result, they not only provide greater durability but also exhibit impressive deformability, establishing a resilient scaffold. Additionally, the continuous and adjustable domain size of BTMs gives engineers an approach to designing porous materials, allowing for permeable control. Therefore, the limitless potential of bijel templated scaffolds makes them incredibly versatile for a wide range of applications within the field of interest.

Despite the remarkable solutions BTMs provide for porous materials, their main challenges lie in processing, selecting suitable polymers, and the limitations imposed by geometry.[17] To solve these issues and expand the spectrum of functional bijel templated materials, a novel approach has been developed. This approach enables the creation of a fully percolating degradable BTM to be used as a bicontinuous mold. The main objective is to introduce desired materials into the pores and induce degradation of the solid channels, resulting in an inverted porous BTM. This degradable material is unique such that any infiltrating substance can be finely tuned to serve as scaffolds in diverse fields like tissue engineering, catalysis, batteries, and fuel cells. Therefore, to expand the current spectrum of functional porous materials, the bijel chemical library must be increased.

1.2 History

In ancient times, dating back to 1500 BCE, the Egyptians cleverly employed charcoal, a porous material, for medicinal purposes.[18] They harnessed its porosity by allowing water to flow through it, extracting nutrients from the substance to alleviate indigestion. This early instance of leaching serves as one of the initial applications that harnessed porous materials in this manner, showcasing their efficacy in nutrient

extraction. Nevertheless, the application of porous materials has since advanced beyond these foundational principles, propelled by their inherent properties, as previously mentioned, to encompass a diverse range of innovative applications. Building upon these concepts, additional interest was sparked in studying liquid-liquid and liquid-gas interfaces, leading to examining binary mixtures and their importance. Researchers can study interfacial interactions through a diverse array of methods. These encompass microscopy techniques[19], measurements of interfacial and surface tension[20], utilization of neutron and x-ray scattering[21], and analysis of rheological properties[22,23], which collectively unveil how fluids interact at their interfaces. Subsequently, researchers can combine these results to engineer materials by applying principles rooted in the foundation of thermodynamics and transport phenomena. This process harnesses the collective potential of common elements, leading to the creation of functional scaffolds with unique morphologies.

In 2005, the team led by Michael Cates at the University of Edinburgh discovered bijels through computer simulations, exploring how colloidal nanoparticles behave within a binary mixture of immiscible fluids. Their aim was to gain an understanding as to the fundamental interactions occurring at the molecular interface through these simulations. These findings highlight a unique effect where nanoparticles kinetically jam the interface between both fluids at their critical composition and halt spinodal decomposition. As a result, these fluids distinctively separate into bicontinuous, fully percolating, non-constricting fluids domains.[24,25] While initial bijel formation in simulations was demonstrated by Dr. Cates' group, another group of experimentalists demonstrated the first experimentally formed bijel using water and 2,6-lutidine in 2007.[26] These results

showed the unique properties of using bijels by selectively tuning their domain size. However, it wasn't until 2010 that Lee and Mohraz pioneered the development of processing techniques to template these bicontinuous fluids into solid scaffolds.[27] As a result, the journey to broaden the current library and functionality of bijel templated materials (BTMs) offers opportunities for porous materials in composite cell delivery hydrogels[12], 3D electrodes for electrochemical energy storage and conversion[28], separation fibers[29,30], and composite eletrolytes[31]. These BTMs provide importance in engineering porous scaffolds with tunable and uniform domain size, structural stability, and continuous morphology.

1.3 Bicontinuous Interfacially Jammed Emulsion Gels

1.3.1 Partial Miscibility

Identifying a system of fluids that are miscible at one temperature and immiscible at another is one of the factors that contribute to bijel formation. Apart from temperature-driven methods, there is also a complementary approach called solvent transfer-induced phase separation (STRIPS) that can form bijels.[32] STRIPS uses fluid composition as the stimulus for phase separation along with surfactant-modified silica where bijel formation depends on relative flow rates, suspension composition, and wetting conditions.[33] However, in the Soft Matter Engineering Laboratory at UC Irvine, some of the work involves developing techniques using temperature transitions on a mixture of partially miscible binary fluids to form bijels. This involves using a silanizing agent to modify the surface of silica nanoparticles to tune surface wettability and stabilize bijels. The preference for using temperature induced phase separation over

STRIPS arises from the distinct spinodal structure evident throughout the entire volume, in contrast to being limited to the edges of a hollow fiber.

The temperature transition method leads a binary system of fluids from a state of miscibility to immiscibility, employing passage through a critical transition temperature. During the process of bijel formation, the system strives to attain its thermodynamically favorable state with the lowest free energy.[34] The temperature transition through the binodal curve is represented by phase diagrams created for binary fluid systems. These diagrams depict phase boundaries correlating a range of compositions at various temperatures under which phase separation occurs. Phase diagrams have revealed the conditions necessary for two immiscible phases to coexist, also known as a miscibility gap.[35] An example system that has been used extensively for bijel templated material applications is water and 2,6-lutidine (W/L). *Reeves et al.* determined the phase diagram for W/L through experimental studies (Figure 1). As the temperature is rapidly raised beyond 34.1°C, at a critical weight fraction of 28% lutidine, the system undergoes phase separate, resulting in the formation of a water-rich phase (Figure 1, “A”) and a lutidine-rich phase (Figure 1, “B”).[36,37] This phase diagram exhibits a concave up curve, indicating a LCST.

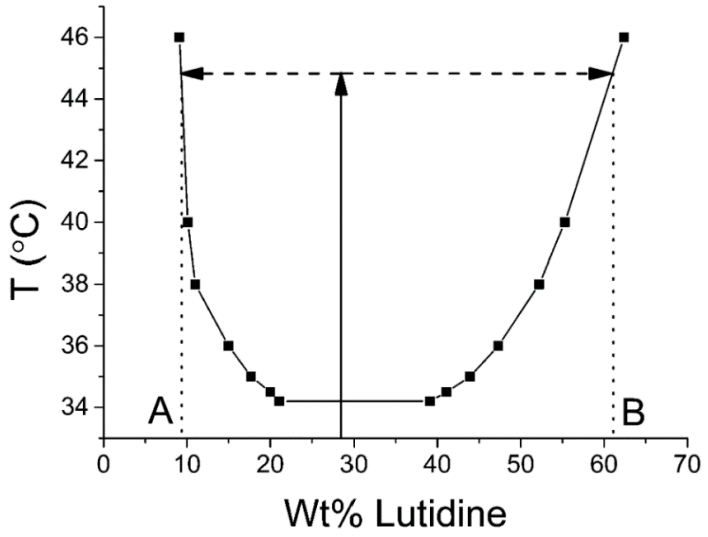

Figure 1: Coexistence curve for Water & 2,6-lutidine.[36]

1.3.2 Spinodal Decomposition

The pathway that contributes to bijel formation is spinodal decomposition in the presence of neutrally wetting nanoparticles, where bicontinuous, interpenetrating fluid domains spontaneously phase separate. The nanoparticles within this system cause the fluids to become kinetically jammed in its spinodal geometry where they prevent coarsening from progressing. Earlier, we discussed the presence of a binodal curve that distinguishes the miscible vs. immiscible state of a fluid system. When the mixture is quenched in temperature, at or close to critical composition, two outcomes are possible: spinodal decomposition, where bicontinuous phase separation occurs, or nucleation and growth, where droplets of one phase form and grow within the other phase.[25] The spinodal regime is illustrated in Figure 2, region I, where rapid temperature quenching at critical composition initiates spinodal decomposition, leading to separation of fluids into compositions of a and b, respectively. Conversely, a small temperature change for a mixture off of critical composition will result in nucleation and growth, where fluid droplets are formed and stabilized by nanoparticles (region II & III, Figure 2). This phase

diagram demonstrates another bijel system composed of ethylene glycol and nitromethane, where a UCST yields similar phase separation into both regions of spinodal decomposition and nucleation.

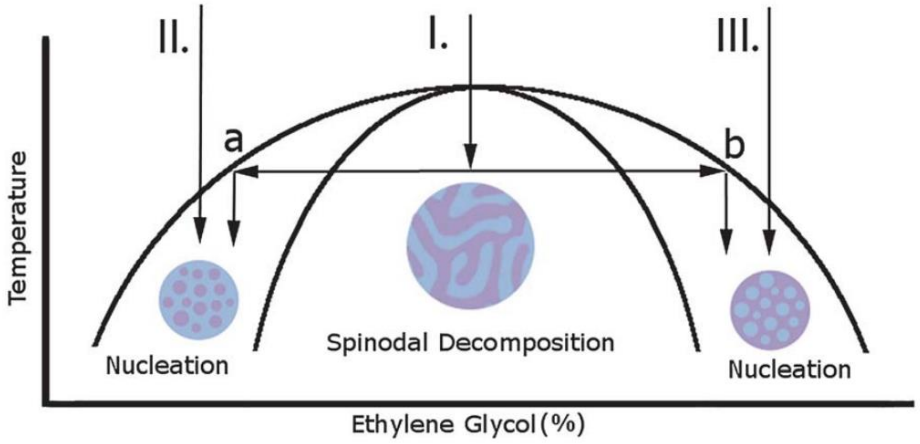

Figure 2: Ethylene glycol & nitromethane coexistence curve demonstrating two quenching pathways for spinodal decomposition (I) and nucleation (II & III).[38]

To determine the spinodal points outlining the spinodal region, Figure 3A displays the initial phase coexistence curve while Figure 3B displays the subsequent free energy curve. These spinodal points exist in regions characterized by inflection points on the free energy curve ($\frac{d^2G}{dX^2} = 0$), designated as S_1 and S_2. These points define the maximum threshold of instability beyond which phase separation cannot be prevented. For example, a starting composition, X_0, quenched rapidly in temperature from T_1 to T_2 will immediately consist of free energy composition, G_0. When a system at point G_0 begins to phase separate in regions of negative curvature ($\frac{d^2G}{dX^2} < 0$), small fluctuations in composition or density will aim to reduce the systems free energy, leading to equilibrium concentrations, X_1 and X_2.[39]

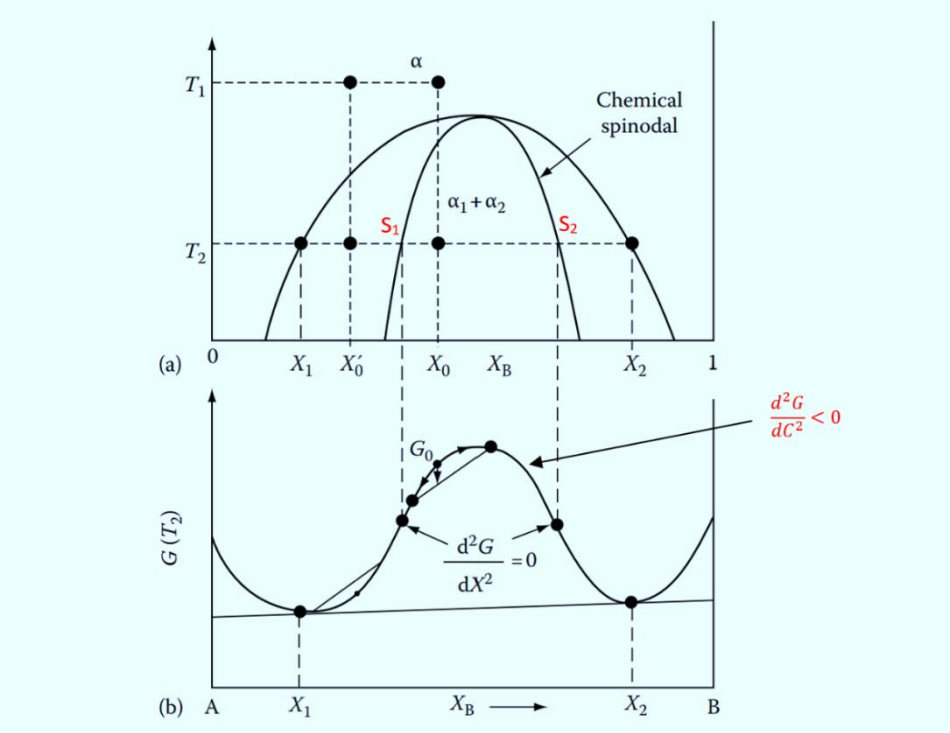

Figure 3: Free energy curve (a) plotted as a function for coexistence curves (b).[34]

Concentration of components are referred to as ‘X’ or ‘C’

The coarsening process through the spinodal region is driven by surface tension, causing it to want to reduce the contact area between two fluids, aiming to minimize free energy. However, it is important to know that phase separation through spinodal decomposition occurs simultaneously throughout the entire volume of the sample. When examined in three dimensions there exist infinite points at the interface between the two fluids with negative Gaussian curvatures, referred to as “saddle points.” Additionally, their unique morphology as interconnected bicontinuous domains is depicted in Figure 4.

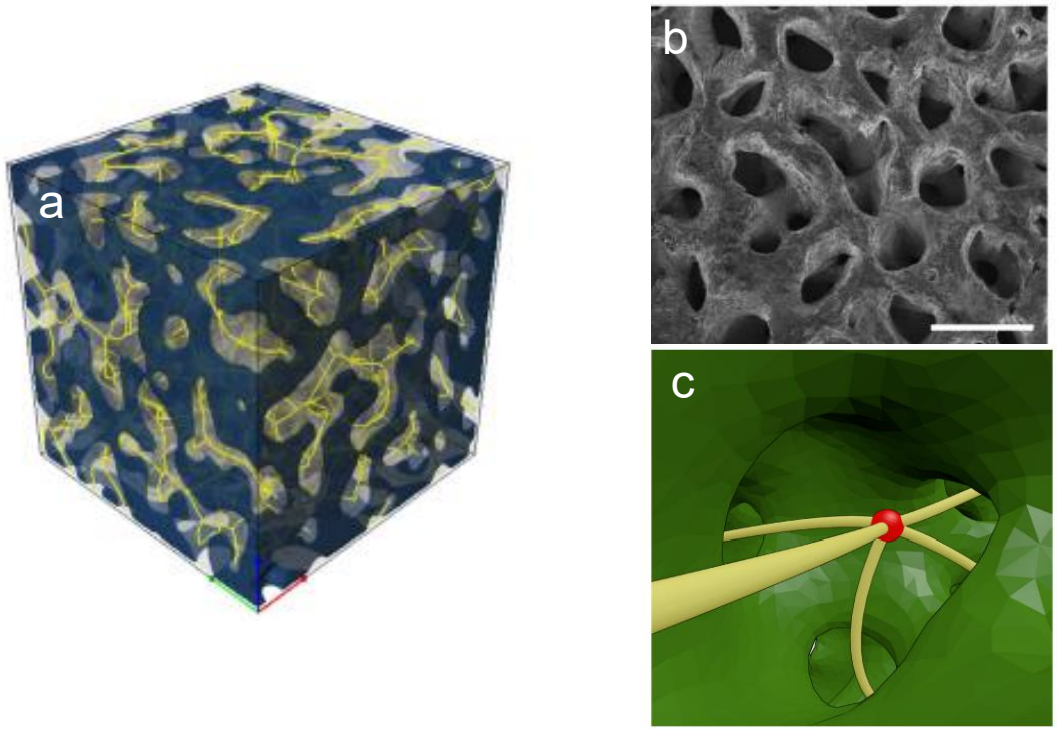

Figure 4: a) 3D construction of μCT data of bijel, grey indicates void whereas blue indicates solid. b) SEM micrograph of polymer bijel, scale bar: 200 μm. c) Illustration of interconnecting point within domains of bijel.[19]

1.3.3 Particle Synthesis and Functionalization

Another significant aspect of creating bijels is the colloidal particles required to jam the interface between two fluids during phase separation. These colloidal particles typically have sizes ranging from 1 nm to 1 μm in diameter and are commonly known as "nanoparticles".[24] They are synthesized using a modified Stöber process where the surface chemistry of monodispersed silica spheres can be tuned to exhibit hydrophilic or hydrophobic properties.[40] The procedure consists of two general steps, first a fluorescent dye is used such as rhodamine B or fluorescein isothiocyanate (RITC or FITC), that covalently binds to a silanizing agent, (3-Aminopropyl)triethoxysilane (APTES). Next, this dye/silanizing agent complex is used

in binding to the surface of the nanoparticles as they react and grow by hydrolysis and condensation. The synthesis of these monodispersed silica particles is accomplished by the following chemical reaction via condensation:

$$Si(OC_2H_5)_4 + 2H_2O \xrightarrow[NH_4OH]{\text{Ethanol}} SiO_2 + 4C_2H_5OH$$

Furthermore, to tune the nanoparticle's affinity to certain fluids, additional silanizing agents may be added during synthesis to modify its wettability. This is necessary for the jamming of these bicontinuous gels because the nanoparticles must be considered neutrally wetting to both fluids in the binary system. This condition results in a preferred spinodal curvature in the liquid interface during jamming. If these particles are not neutrally wetting, the curvature of the domains leads to pinch-off events, destroying connectivity of the spinodal microstructure.[25] The term, "wettability," is measured through a three-phase contact angle (θ) that yields a hydrophilic or hydrophobic interaction with its surrounding environment. A hydrophilic contact angle exists where $0° \leq \theta < 90°$ and the nanoparticles preferentially favor the water (or alcohol phase), while a hydrophobic contact angle $90° < \theta \leq 180°$ allows nanoparticles to favor the oil (or organic) phase (Figure 5). To favor both fluids equally and jam the interface, these nanoparticles must sit at 90° and sustain a net-zero curvature at the fluid-fluid interface.[17,19] Over time, the fluid domains will coarsen until the interfacial area is reduced to reduce the total energy of the system, contributing to the jamming that is characteristic of a bijel (Figure 6).

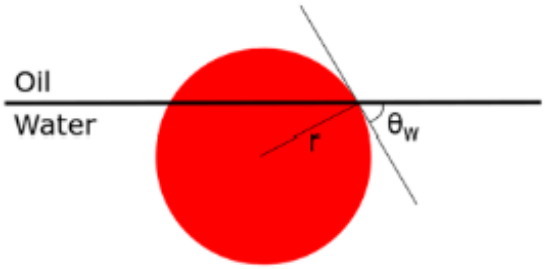

Figure 5: a) Contact angle (θ_w) at the liquid-liquid interface with particle of radius r.[25]

Bijels naturally inherit a tunable domain size (ξ) solely due to the particle volume fraction (ϕ) and particle diameter (d).[26] At a fixed volume fraction, smaller diameter particles will require less interfacial area to be incorporated, yielding smaller domains. Transversely, particles of the same volume fraction, now with a larger diameter, will require more interfacial area to occupy the interface, resulting in larger domains.[25] If you consider tightly packed spheres with monolayer coverage of spherical particles, the equation for domain size can be derived (Equation 1). Thus, the size of the fluid domain is inversely proportional to the particle volume fraction (ϕ ~ 0.5%- 4.0%).

$$\xi = \left(\frac{\pi}{\sqrt{3}}\right)\left(\frac{d}{\phi}\right) \qquad \text{Equation 1}$$

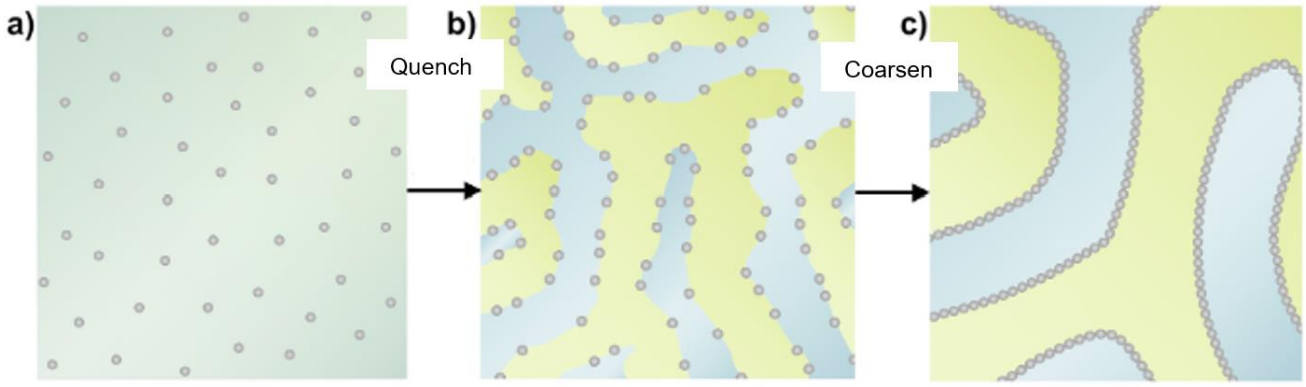

Figure 6: Bijel formation schematic.[9] a) Neutrally wetting particles dispersed in binary fluid system at critical composition. b) Raising the system past its transition temperature prompts spinodal decomposition, neutrally wetting particles start to line the fluid-fluid interface. c) Coarsening of particles continues until the system becomes jammed and the interface is fully occupied by particles.

1.4 Bijel Templated Materials

One of the major drawbacks of bijels and bijel processing is the methods used to template these structures into feasible scaffolds. In 2010, *Lee and Mohraz* developed a processing route to use these interpenetrating bicontinuous phases as a template into polymeric 3D porous geometries. This involved adding a monomer of interest on top of an arrested bijel and allowing it to diffuse downward throughout the sample.[27] In this method, bijels are incubated above their transition temperature, and a photopolymerizable monomer (or polymer) is added on top of the mixture, allowing selective partitioning into one of the fluid phases. This approach of processing BTMs enables precise control over the final polymer crosslinking density by specifying both the quantity and composition of polymer introduced to the system. To fulfill this purpose, a diverse range of monomers can be utilized; however, two criteria must be satisfied: i)

the chosen monomer should exhibit selective miscibility with the organic phase (2,6-lutidine) in the bijel, and ii) it must possess the ability to undergo crosslinking through radical polymerization under UV light. While the process of replacing a fluid phase with a monomer offers significant benefits for solidifying these bijel structures into solid materials, it's important to acknowledge certain limitations. First, the incorporation of a monomer in place of a fluid phase can be time-consuming, spanning several hours. Second, the reliance on mass transfer kinetics during this process imposes constraints on the attainable sizes and shapes of these BTMs. Additionally, it's worth noting that bijels are kinetically jammed and influenced by the surface tension of their environment. Introducing a third component, such as a monomer, to the fluid mixture may impose gravitational stress and additional interfacial stress within the system, which could result in a deformed microstructure or hinder the selective partitioning during the solvent-monomer exchange process.[17]

1.4.1 Water/2,6-Lutidine System

Of the bijel systems published and commonly employed, the water/2,6-lutidine (W/L) system has demonstrated high feasibility with respect to bijel processing. For this system, fluorescent silica particles with an average diameter of 500 nm were synthesized using a modified Stöber process where APTES is conjugated to rhodamine B as a fluorescent dye.[27] In the course of particle growth, the dye/APTES complex is introduced to modify the surface of the particles. To achieve a 90° contact angle, particles were dried under vacuum (-25 inHg) at 135°C until they reached neutrally wetting behavior.[9] A Confocal Laser Scanning Microscopy (CLSM) image of a bijel

formed using the W/L system is shown with neutrally wetting particles lining the fluid-fluid interface (Figure 7).

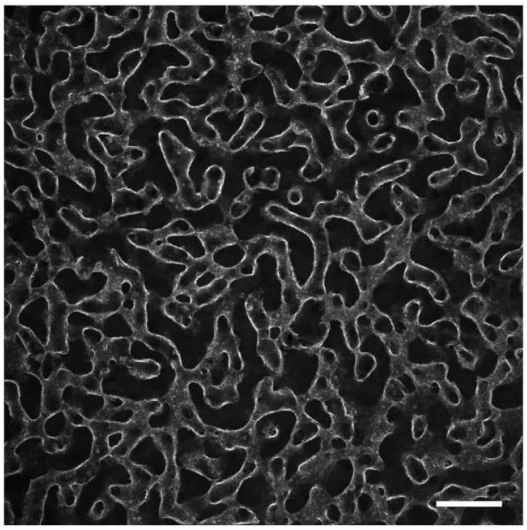

Figure 7: CLSM image of W/L bijel. Bright and dark phases indicate water and 2,6-lutidine, respectively, where nanoparticles line the interface.[19] Scale bar: 100 μm

In this processing method, monomer casting is used with these bicontinuous structures as a template to convert them into workable scaffolds.[12] Prior to raising the particle, water, and lutidine mixture through its transition temperature, the mixture can be placed into a cylindrical glass tube with an inner diameter of 5 mm, securely attached to a glass coverslip using polydimethylsiloxane (PDMS) as an adhesive. Electromagnetic radiation in the form of microwaves is used to heat the sample past its transition temperature to initiate spinodal decomposition and bijel formation. Samples are then incubated in an oven at 70 °C, above the transition temperature, to keep the particles stabilized at the fluid-fluid interface for processing. A premade solution of an acrylate-based monomer with a photoinitiator is subsequently pipetted on top of the bijel. After several hours, the sample is exposed to UV light using an integrating sphere,

ensuring uniform irradiation throughout its volume (Figure 8). Subsequently, the sample undergoes washing in ethanol and water, followed by dying in an oven for future use.

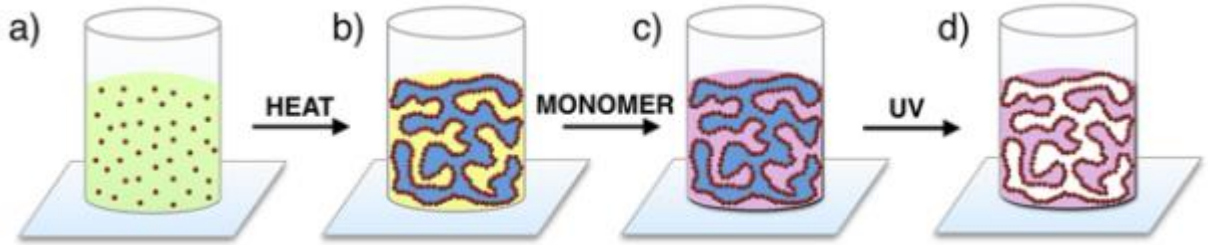

Figure 8: Schematic of bijel templating process.[12] a) Nanoparticles are suspended in a mixture of W/L at critical composition and placed into a cylindrical glass tube. b) Sample is heated above the transition temperature. c) Monomer with photoinitiator is added on top and allowed to diffuse down. d) UV irradiation to polymerize the sample

1.4.2 Intrinsically Polymerizable Bijels: 1*,4-Butanediol/PEGDA System*

In a recent breakthrough, *Ching et al.* created a novel technique in 2021 that enables the direct creation and templating of bijels by choosing a monomer as one of the fluid phases.[17] This approach called intrinsically polymerizable bijels (IPBs) was created as a solution to overcome the limitations mentioned with monomer casting, enhancing the processing capabilities of BTMs. Upon phase separation and quenching the fluids past their transition temperature, a bicontinuous monomer-rich phase and a monomer-poor phase develop. Through the addition of colloidal particles with precisely tuned surface chemistry aligning that of the two fluids, particles favor both fluids equally and achieve a neutrally wetting state. From this, particles adopt a 90° contact angle with equal affinity to both fluids, causing them to sit at the fluid interface. When this mixture undergoes sonication, causing its temperature to rise above its UCST, and is then quickly cooled through its miscibility gap, it undergoes spinodal decomposition, resulting

in the jamming of particles at the fluid interface. Therefore, after phase separation, photopolymerization selectively solidifies one of the two phases, converting bijels into BTMs.

In the IPB system, a combination of two components is used together to create a porous scaffold, a quencher that selectively partitions into the alcohol phase and a photoinitiator that selectively goes into the monomer phase. Phase separation does not yield 100% pure fluids but instead leads to a monomer-rich phase and a monomer-poor phase, where exposure to UV light can cause both phases to solidify at different densities, resulting in a non-porous scaffold. To overcome this obstacle, a fluorescent dye is used as a photon quencher. This dye selectively favors the monomer-poor (alcohol) phase, locally quenching photons and preventing polymerization, creating a porous scaffold. This processing technique not only resolves the limitations of the monomer casting method but opens the door to scalable processing of BTMs, thereby unlocking novel possibilities for the creation of advanced materials.

The development of a self-polymerizing bijel system, capable of undergoing polymerization intrinsically has opened new opportunities. One of the first IPB systems developed was 1,4-butanediol (BD) and poly(ethylene glycol) diacrylate (PEGDA) (M_n: 250 g mol $^{-1}$) where cloud point analysis was used to create the phase diagram. The determined critical composition was 47.5% BD and 52.5% PEGDA by volume with an UCST of 48.7 °C (Figure 9).

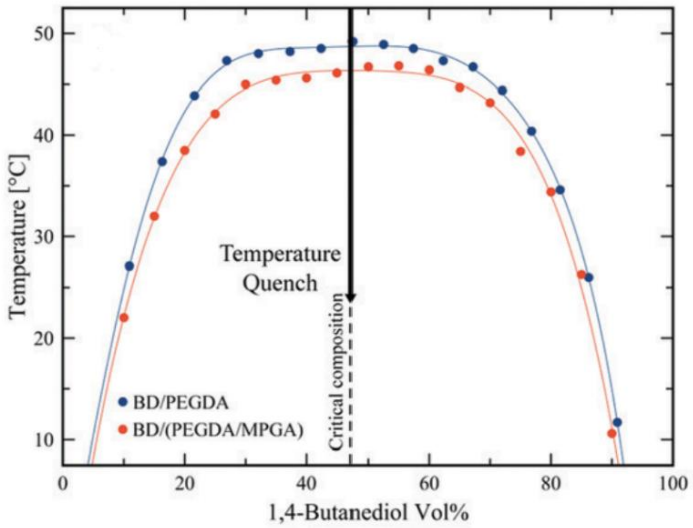

Figure 9: Coexistence curve of 1,4-butanediol and PEGDA 250.[17]

Neutrally wetting nanoparticles were synthesized for the BD/PEGDA 250 system with hexamethyldisilazane (HMDS) as a silanizing agent to impart hydrophobic properties by introducing methyl groups onto the silica's surface. These nanoparticles were tagged using fluorescein isothiocyanate (FITC) as a fluorescent dye as opposed to rhodamine B isothiocyanate (RITC) and effectively synthesized with an average diameter of 200 nm. This allows bijel to be observed and imaged during formation using CLSM (Figure 10).

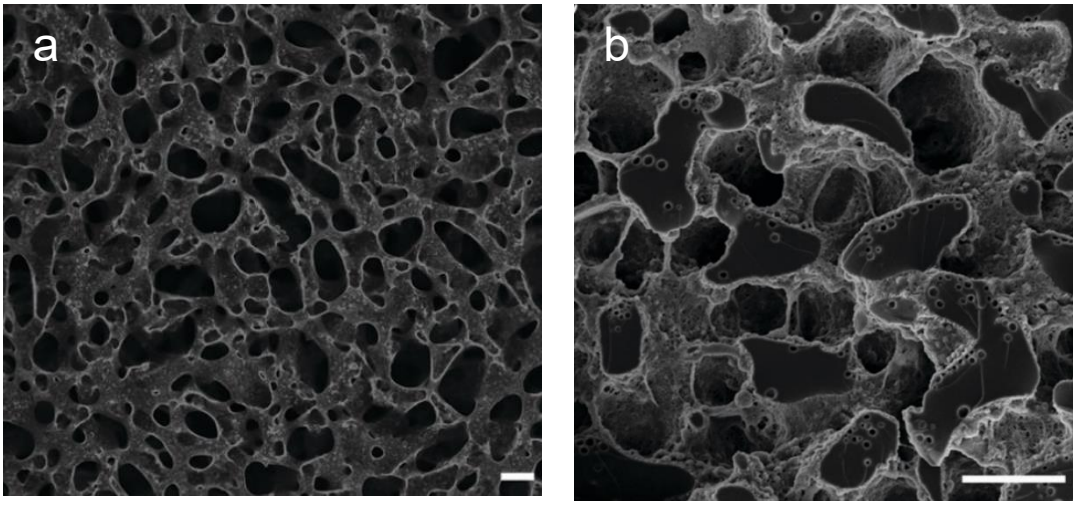

Figure 10: a) BD/PEGDA 250 bijel observed via CLSM (Scale bar: 40 μm).[17] b) SEM image of BTM using selective photon quenching (Scale bar: 40 μm)

Selective photon quenching of the monomer-poor region was used so that a porous phase is developed post polymerization. Additionally, it is crucial to carefully choose a photoinitiator with a strong affinity to the monomer-rich phase while simultaneously incorporating a photon quencher that selectively diffuses into the monomer-poor phase (BD phase). In this case, DMPA (1.87 mM) and sodium fluorescein salt (0.14 mM) were chosen, respectively.[17] The relative fluorescence and absorption spectra of both fluorescein and DMPA dissolved in the monomer-poor phase were compared, leading to the selection of an initiation wavelength. This wavelength ensures that photons are absorbed in the alcohol-rich phase, preventing polymerization, while maintaining enough DMPA in the monomer-rich phase for polymerization under low intensity.

Through local photon quenching, UV polymerization can then be carried through to template intrinsically polymerizable bijels into BTMs. This process can be summarized by creating a bijel mixture composed of both fluids, neutrally wetting

particles, and a photon quencher, placing the mixture into a PDMS mold, quenching, and flashing with UV (λ=320-390 nm) (Figure 11).

Figure 11: Schematic representation of intrinsically polymerizable bijels (IPB)

1.5 Summary

Developing a novel category of porous materials with broad applicability across diverse research domains has become a matter of great significance. As such, finding binary fluids with partial miscibility is the first step in aiming to develop a bijel. Next, creating a phase diagram that delineates the spinodal region from the nucleation region becomes crucial for comprehending both the critical composition and temperature of the fluids. Therefore, to jam the interface and kinetically halt spinodal decomposition, neutrally wetting nanoparticles must be synthesized to equally favor both fluids and sit at the interface. To solidify these bicontinuous architectures into 3D porous scaffolds, a monomer casting method can be used to replace one of the fluid phases. However, limitations of this approach exist, giving scalability issues, geometric constraints, and imposing additional stress on bijels, ruining their microstructure. As a result, IPBs were created to directly polymerize one of these bijel phases into 3D geometries using selective photon quenching. Using these techniques, researchers can begin to develop novel bijel systems and broaden the range of functional bijel materials. The content detailed in Chapter 1 lays the groundwork, encompassing theoretical concepts and

earlier instances of bijel and BTM development, setting the stage for the novel research I conducted in Chapter 2 and 3 pertaining to IPBs and degradability.

Chapter 2. Expanding Bijel Chemical Library

2.1 DSDA/1,2-Pentanediol System

2.1.1 Introduction

Degradable materials have emerged to be an appealing field of interest for research and development, attracting attention across various disciplines of science and engineering. These materials harness the ability to undergo controlled degradation allowing for advantages and opportunities in biomedical engineering[41], catalysis[42], environmental sustainability[43], and beyond. In the area of biomedical engineering, degradable scaffolds play a pivotal role in the advancement of drug delivery systems, tissue engineering scaffolds, and biodegradable implants.[44,45] Therefore, having the ability to control and degrade within the body over time provides crucial benefits, including reduced inflammation and enhanced tissue regeneration. Within the field of catalysis, a material that can control the kinetics of a reaction based off the release of an active species plays a crucial role in efficient product formation. Furthermore, applying degradable materials as a sustainable option to reducing non-degradable waste holds immense promise in the field of environmental sustainability. To engineer a bijel using the IPB method, a degradable monomer can be incorporated into one of the bicontinuous phases, opening various applications in the fields previously mentioned.

Building upon the principles published in Ching and Mohraz's (2021) work, a novel approach was proposed utilizing a monomer of a similar structure to that of

PEGDA. It is commonly known that compounds containing disulfide bonds can undergo degradation in the presence of a reducing agent in proper conditions.[46–49] Taking this into consideration, a disulfide containing diacrylate based monomer, referred to as DSDA (disulfide diacrylate) or bis(2-acryloyloxyethyl) disulfide, was successfully synthesized.[50] This compound shares a similar structure to PEGDA but now contains a disulfide bond, allowing the ability to degrade and expand its potential application. An extensive research investigation was conducted to identify a partially miscible counterpart to DSDA. Subsequently, colloidal particles with specific surface chemistry were synthesized to line the interface between the two fluids during demixing at their critical composition. Quenching this particle-fluid mixture through its critical temperature at the critical composition allows the mixture to undergo spinodal decomposition and form a bijel. However, to solidify this bijel into a 3D porous scaffold, selective photon quenching must be successfully determined for this system.

The novel development of a degradable BTM paves the way for the creation of an inverted bicontinuous scaffold, which can serve as a templated mold for infiltrating voids with diverse materials, followed by solid phase degradation. This breakthrough opens a vast array of material possibilities, facilitating the incorporation of spinodal structures into scaffolds and driving advancements in material science and microstructural engineering.

2.1.2 Materials

The following chemicals were used as received. 1,2-Pentanediol (96%), 2-hydroxyethyl disulfide (technical grade), triethylamine (≥ 99.5%), acryloyl chloride (≥ 97%), 3-(Trimethoxysilyl)propyl methacrylate (TMSPM, 98%),

(3-Aminopropyl)triethoxysilane (APTES, 99%), fluorescein isothiocyanate isomer I (FITC, ≥ 90% HPLC, powder), and silica gel (high-purity grade, average pore size 60 Å, 70-230 mesh, 63-200 µm, for column chromatography) was purchased from Sigma-Aldrich. Sodium sulfate (anhydrous, granular), basic alumina (60-325 mesh), ammonium hydroxide (28-30%), 2-propanol, acetonitrile, and methylene chloride were purchased from Thermo Fisher Scientific. Poly(dimethylsiloxane) (PDMS) was purchased from Dow Corning. 3-methoxypropyltrimethoxysilane was purchased from Gelest. Fluorescein sodium salt was purchased from HiMedia Laboratories. Chloroform (HPLC grade) was purchased from J.T. Baker. Ethyl alcohol (200 proof) was purchased from Gold Shield.

2.1.3 DSDA Synthesis

A nucleophilic addition-elimination mechanism in the reaction between 2-hydroxyethyl disulfide (24.6 g, 1 equiv, 159.88 mmol) and acryloyl chloride (32.3 ml, 2.5 equiv, 399.7 mmol) with triethylamine (45 ml, 2 equiv, 319.76 mmol) as a base was used to synthesize the DSDA (Figure 12). All components were added to a one liter round bottom flask with chloroform (400 ml) as a solvent. The flask was then stirred and cooled to 0 °C under Argon, followed by the gradual addition of acryloyl chloride (32.3 ml, 2.5 equiv, 399.7 mmol) dropwise. The reaction was stirred for 24 hours and left to warm to room temperature overnight. The solvent was evaporated under reduced pressure, resulting in the collection of the byproduct salt, which was filtered and washed with methylene chloride (DCM). The solution was then washed 6 times with an aqueous sodium carbonate solution (Na_2CO_3, 0.1 M) in a separatory funnel and dried over granular sodium sulfate (Na_2SO_4). To gather the crude product, the solvent was

evaporated under reduced pressure to yield a brown oil. Isolation of DSDA began by packing a column with basic alumina using DCM as an eluent, transferring the crude product on top, and passing it through to yield a colorless oil (159.88 mmol).[50] Structure of DSDA was confirmed through H NMR analysis where proton peaks match with respect to *Zhao et al.* (Figure 13). Further isolation through silica gel (70-230 mesh size, 63-200 μm) using DCM was conducted to remove all remaining byproducts and ensure purity for proper cloud point analysis. For large-scale production, a 2.5x scale-up of DSDA was performed using the same workup and isolation procedures, resulting in 49.21 grams of pure material with a 72.33% yield.

Yield: 32.83 g, 78.28%. H NMR (400 MHz, $CDCl_3$, δ, ppm): 2.97 ppm t (4H), 4.41 ppm t (4H), 5.85 ppm d (2H), 6.14 ppm q (2H), 6.41 ppm d (2H).

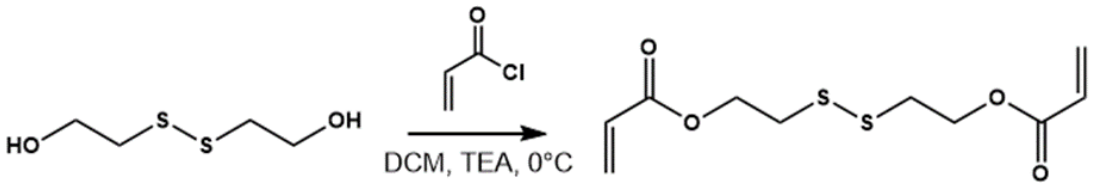

Figure 12: Chemical illustration of DSDA reaction

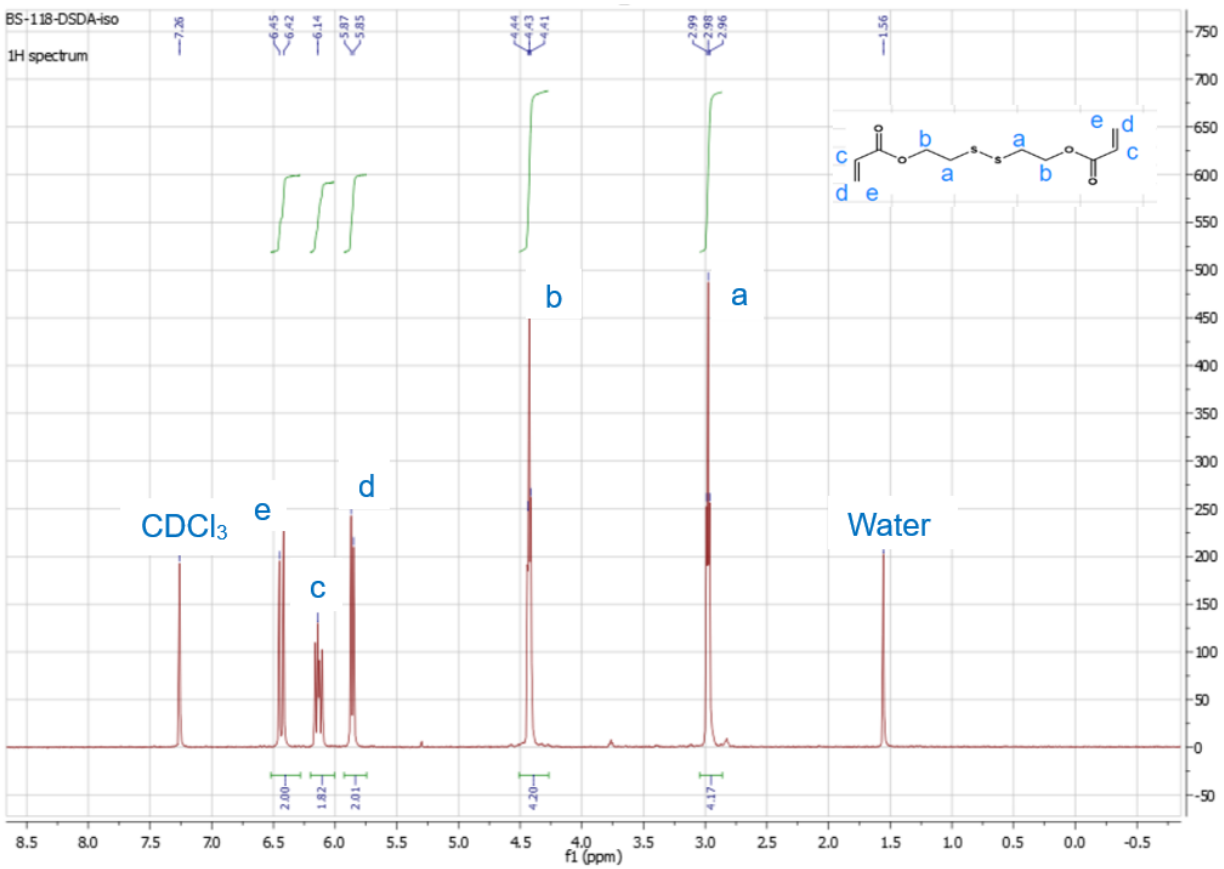

Figure 13: H NMR of DSDA after isolation, $CDCl_3$ used as a solvent. Letters (a-e) represent corresponding hydrogens on DSDA's carbon chain.

2.1.4 Discovering a Partially Miscible System with DSDA

In the search for an alcohol that exhibits partial miscibility with DSDA, a range of alcohols were screened to identify the most suitable candidate. Alcohols that contained diols with short to medium carbon chains were mixed with DSDA at 50% volume fraction at room temperature, heated above (80 °C) and cooled below (0 °C) room temperature to qualitatively see if partial miscibility existed at a workable range. The following diols were screened: ethylene glycol, 1,2-propanediol, 1,3-propanediol, 1,2-butanediol, 1,2-pentanediol, and 1,5-pentanediol. Among these alcohols, 1,2-pentanediol demonstrated miscibility at room temperature but underwent transition at 0 °C, while 1,2-butanediol

and 1,2-propanediol exhibited a transition to a miscible state at elevated temperatures. Further investigation via cloud point analysis was carried out to map the phase diagram via turbidity measurements. Both 1,2-propanediol and 1,2-pentanediol exhibited a UCST with 1,2-pentanediol transitioning at a lower temperature (Figure 14). Inherently, full mapping of the DSDA/1,2-pentanediol phase diagram was completed and bijel analysis was thoroughly sought out.

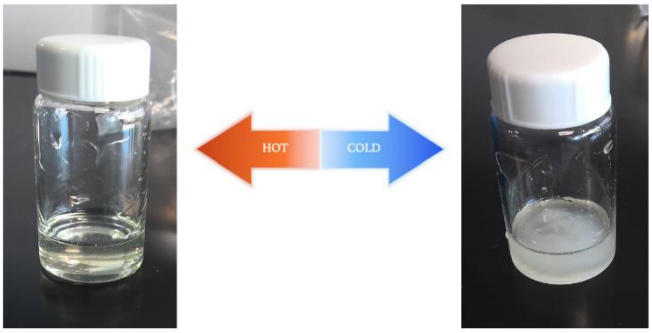

Figure 14: Initial testing to determine partial miscibility of DSDA to 1,2-pentanediol at room temperature (Hot) and cooled on ice (Cold)

2.1.5 Phase Diagram: DSDA/1,2-Pentanediol

A comprehensive phase diagram was experimentally determined by conducting cloud point measurements with a 488 nm laser (Mells Griot, Model no: IMA101040ALS) under a constant current. A schematic of the turbidity setup shown below uses a laser, negative and positive lenses, a temperature-controlled ethanol bath, a stir plate, a thermistor, and a photodiode (Figure 15). Within the lens setup, a concave-plano lens expands the laser beam to increase the probability of interacting with points of turbidity within the sample in a glass optical cuvette (Macro Cell, 10 mm light path). This cuvette is placed inside a temperature-controlled ethanol bath (Julabo CF41) where the

temperature can be controlled at increments of 0.5 °C while being stirred. A convex-plano lens then focuses the transmitted beam onto a silicon photodiode (ThorLabs, 400 ns rise time). The voltage read is then correlated to the intensity of the laser beam and passed through a myDAQ, transmitting measurements to our LabView software along with the temperature of the solution via the transistor.

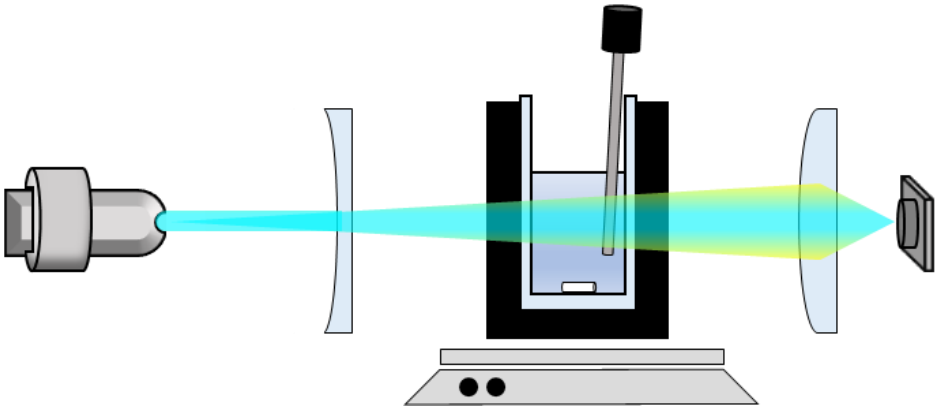

Figure 15: Schematic of turbidity, cloud point measurement set up.

To first calibrate the intensity of light transmittance as well as monomer purity, a constant voltage was supplied through 100% DSDA placed in the cuvette at temperatures ranging from 20 °C to 70 °C. This was to ensure no voltage change was recorded over the experimented temperature range (Appendix A1). For each experiment, a solution of DSDA to 1,2-pentanediol (1,2-PD) was mixed at respective mass fractions ranging from 90% DSDA to 20% DSDA and added to the cuvette. The temperature was slowly cooled (0.5 °C min^{-1}) from 20 °C to 0 °C to find the transition temperature of each respective mass fraction mixture. Each temperature cooling experiment was performed three times and cloud point measurements were determined using a Matlab script where the inflection point of a voltage vs temperature plot would yield the transition temperature (Appendix A2). This value was averaged across all three cooling experiments and plotted over a compositional range of 90% DSDA to 20%

DSDA. The binodal curve was calculated by fitting a third order Fourier series through the averaged experimental values. A critical mass fraction of 54% DSDA to 46% 1,2-PD at a critical transition temperature of 14.28 °C was then extrapolated from the fitted curve (Figure 16).

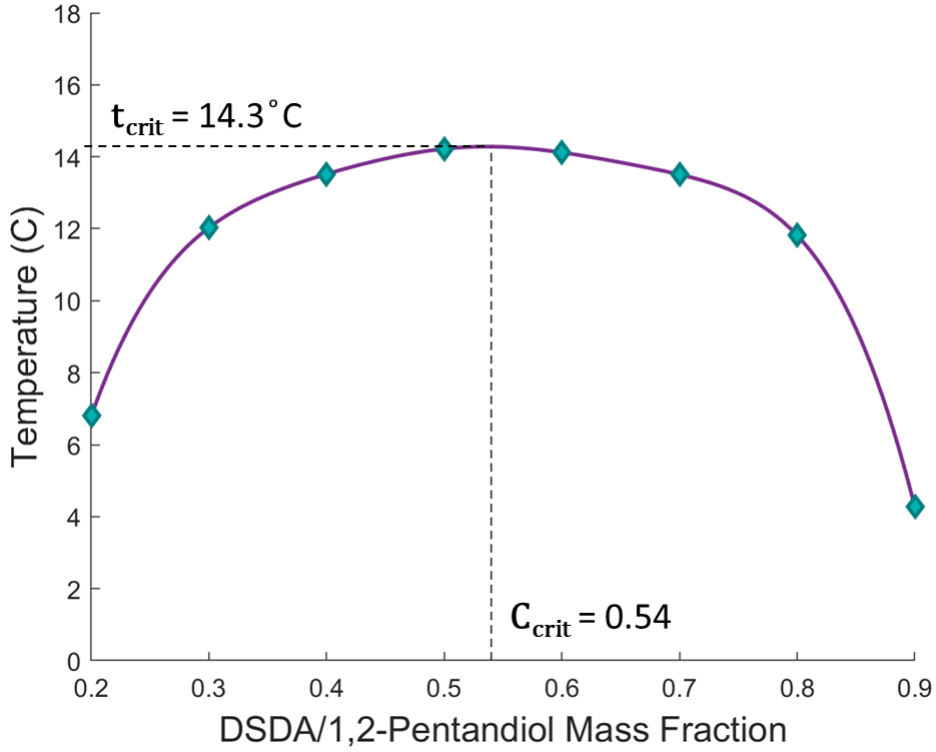

Figure 16: Coexistence curve of DSDA/1,2-PD determined via cloudpoint analysis.

2.1.6 Functionalized Silica Nanoparticles & Bijels

For bijels to form, there's a critical component of neutrally wetting nanoparticles required to line the fluid-fluid interface. These particles can be made in multiple ways to yield different wettability based on the type of silanizing agent used to decorate the surface of silica. The synthesis process discussed earlier for the water/2,6-lutidine system requires using APTES to functionalize the surface while also requiring cumbersome oven tuning mixed with periodic and frequent wettability testing. Even

though this was the case, these particles were first attempted with the DSDA/1,2-PD system and jammed the fluid-fluid interface during spinodal decomposition, forming a bijel (Figure 17).

Bijel formation and phase separation was imaged using an inverted microscope equipped with a VT-Infinity confocal scanner from VisiTech International. A small metal block cooled to 0 °C was used to maintain the sample's temperature during imaging on a Zeiss microscope equipped with a 10x objective (10x/0.25 N-ACHROPLAN lense). Images of the bijel were observed on a computer where a sodium fluorescein salt, previously mixed with the 1,2-pentanediol, is observed as the bright phase, whereas the DSDA is observed as the dark phase, separated by colloidal particles at the fluid-fluid interface.

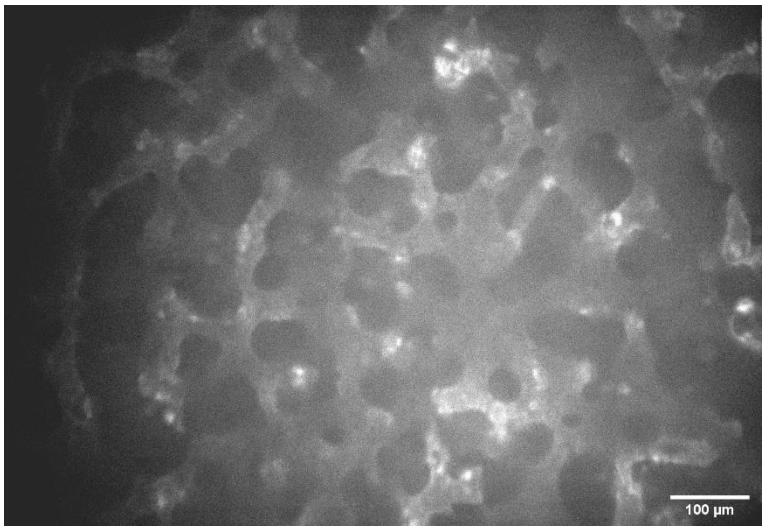

Figure 17: First DSDA/1,2-PD bijel using silica nanoparticles functionalized with APTES.

Alternative silanizing agents and implementation of a slightly modified protocol was explored to reduce the need for intensive tuning required with APTES functionalized silica nanoparticles. With this objective in mind, we selected three

candidates for this approach: hexamethyldisilane (HMDS), 2-(carbomethoxy)ethyltrimethoxysilane (2CMETS), and 3-(trimethoxysilyl)propyl methacrylate (TMSPM).

The first candidate, HMDS, is a silanizing agent that adds methyl groups to the surface of silica upon functionalization, shifting the wettability to be hydrophobic. The synthesis began by using a 20 mL glass scintillation vial inside of a humidity-controlled glove box ($RH < 15\%$) stored under nitrogen. In the vial, 16.65 mg of fluorescein isothiocyanate (FITC) was conjugated to 70.3 µL APTES in 13.32 g of anhydrous ethanol and stirred for 1 hour to create a FITC/APTES dye complex. Next, to each of the nine vials, 10.0 g of ethanol, 1.25 mL of deionized water, 1 mL of FITC/APTES dye, 680 µL of tetraethyl orthosilicate (TEOS), and 290 µL of ammonium hydroxide were added, stirring at room temperature for 5 hours. Varying volume fractions of HMDS (ϕ_{HMDS}) ranging from 5.3 x 10^{-3} to 1.0 x 10^{-2} were added evenly across 9 vials. The growth and surface functionalization of these nanoparticles were allowed to stir for 18 hours at room temperature. Particles were washed by repeated cycles of suspension, centrifugation at 5000 rpm for 10-minutes, and supernatant drainage for three cycles in ethanol, and once in water before being dried at 75 °C for 1 hour, creating particles with an average diameter of 200 nm. The particles exhibited selective partitioning into the 1,2-PD phase, showing that they were not neutrally wetting. This was confirmed by sonicating particles in a DSDA/1,2-PD mixture, where the respective fluid densities were 1.19 g mL^{-1} and 0.971 g mL^{-1}, where upon settling, the particles favored the 1,2-PD phase (Figure 18).

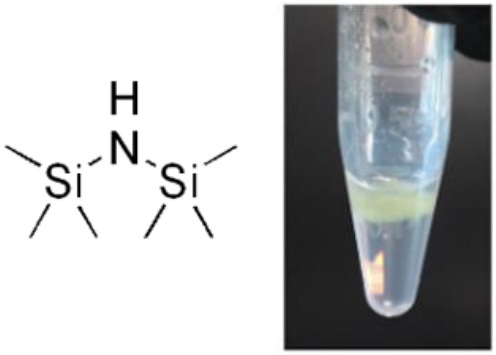

Figure 18: HMDS structure illustrated with functionalized particles sitting in the 1,2-pentanediol phase (top) upon settling.

Based on the results from the HMDS examination, we chose the two additional candidates based on the functional group's similarities to DSDA in hopes of shifting the particle wettability towards favoring DSDA. The synthesis of 2CMETS functionalized nanoparticles followed the same method as before, but this time, volume fractions (ϕ_{2CMETS}) ranging from 9.07 x 10^{-3} to 15.0 x 10^{-3} were evenly added across 9 vials. Both an illustration and an image of the functionalized surface and size distribution are further shown (Figures 19 & 20).

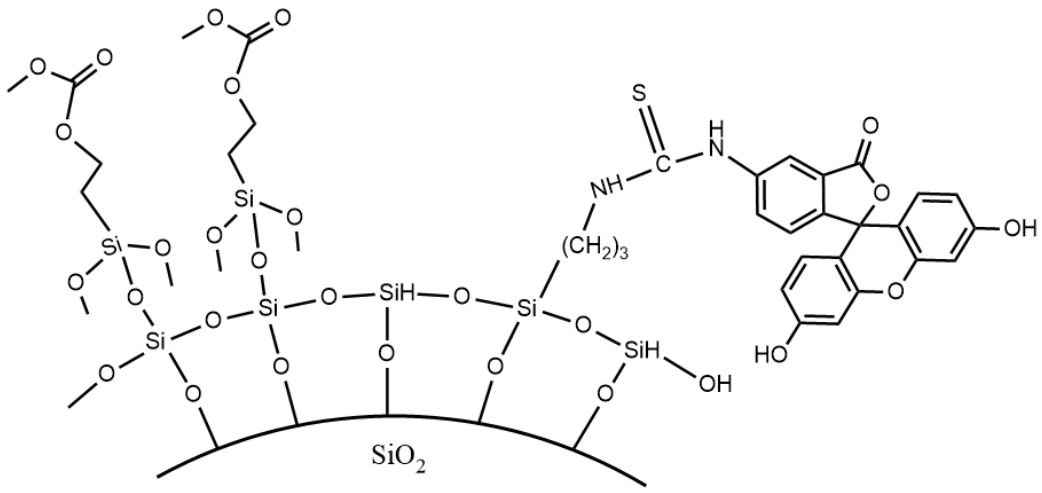

Figure 19: Surface chemistry of silica nanoparticles with 2CMETS and FITC/APTES dye complex

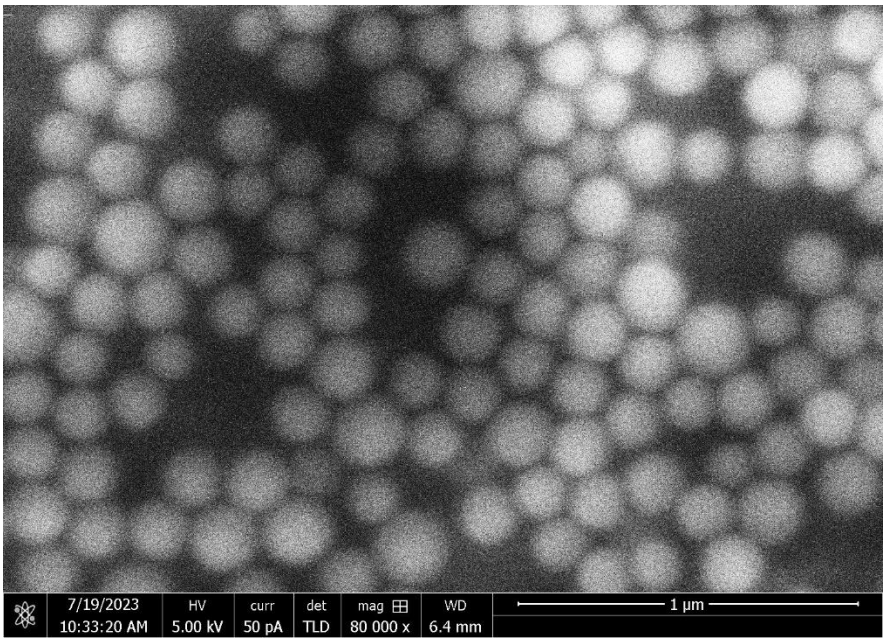

Figure 20: SEM of 2CMETS silica nanoparticles with an average diameter ~ 186 nm

Upon drying these particles, neutral wettability was determined by successful bijel formation, imaged through via CLSM. First, an ultrasonic horn (Branson Sonifier 250) was used for 30 seconds to effectively disperse 2.5 mg of silica particles in 128 mg of DSDA. The mixture was returned to a scale, and a premade solution of 1,2-pentanediol and sodium fluorescein salt (0.1 mM) was added to achieve a critical mass fraction of 54% DSDA. The solution was effectively homogenized through 20 seconds of vortex mixing and 5 minutes of sonication. The mixture was gently transferred into preheated (70 °C) capillaries (0.40 mm x 8.00 mm I.D., Vitrocom), allowed to heat for 1 minute, then quickly quenched on an aluminum block placed in a bath of dry ice and acetonitrile. The bijel sample was quenched for approximately 1 minute on the -40 °C cooled aluminum block before being transferred to a 0 °C aluminum block in an ice bath for the sample to slowly heat up for fluorescent imaging while still remaining under its UCST. Imaging each of the nine 2CMETS functionalized nanoparticles revealed a

nonmonotonic variation as the volume fraction of silanizing agent (ϕ_{2CMETS}) increased for each of the samples immediately upon synthesis (Figure 21). When these particles were stored in a dark environment over time, their surface chemistry shifted to become more neutrally wetting (Figure 22). Particles sustained their neutrally wetting properties over 8 days, whereas the dynamic surface of APTES functionalized nanoparticles change wettability day by day.

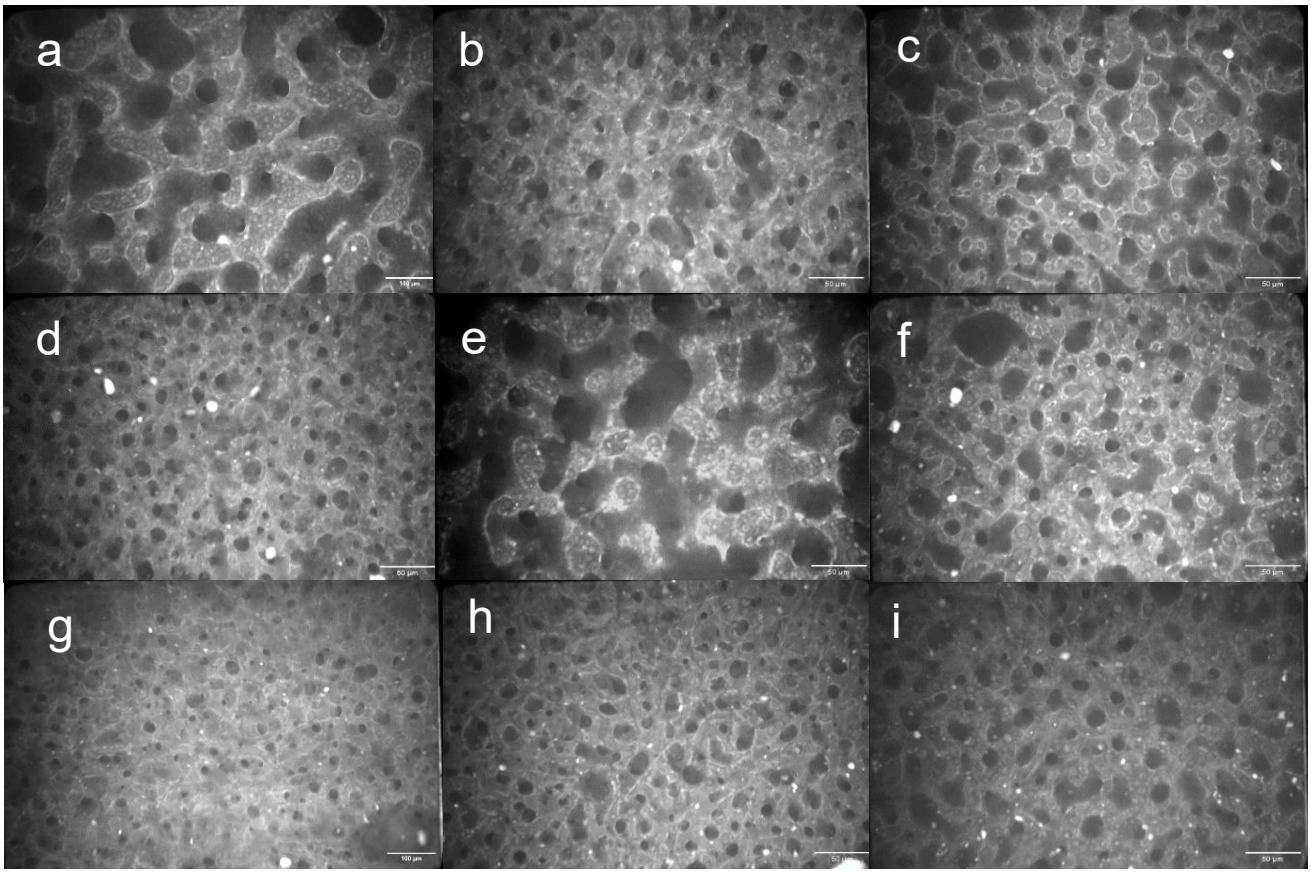

Figure 21: 2CMETS bijels checked immediately upon synthesis.

a) $\phi_{2CMETS} = 9.07 \text{ x } 10^{-3}$ b) $\phi_{2CMETS} = 9.82 \text{ x } 10^{-3}$ c) $\phi_{2CMETS} = 10.6 \text{ x } 10^{-3}$

d) $\phi_{2CMETS} = 11.3 \text{ x } 10^{-3}$ e) $\phi_{2CMETS} = 12.1 \text{ x } 10^{-3}$ f) $\phi_{2CMETS} = 12.8 \text{ x } 10^{-3}$

g) $\phi_{2CMETS} = 13.5 \text{ x } 10^{-3}$ h) $\phi_{2CMETS} = 14.3 \text{ x } 10^{-3}$ i) $\phi_{2CMETS} = 15.0 \text{ x } 10^{-3}$

Scale bar = 50 μm

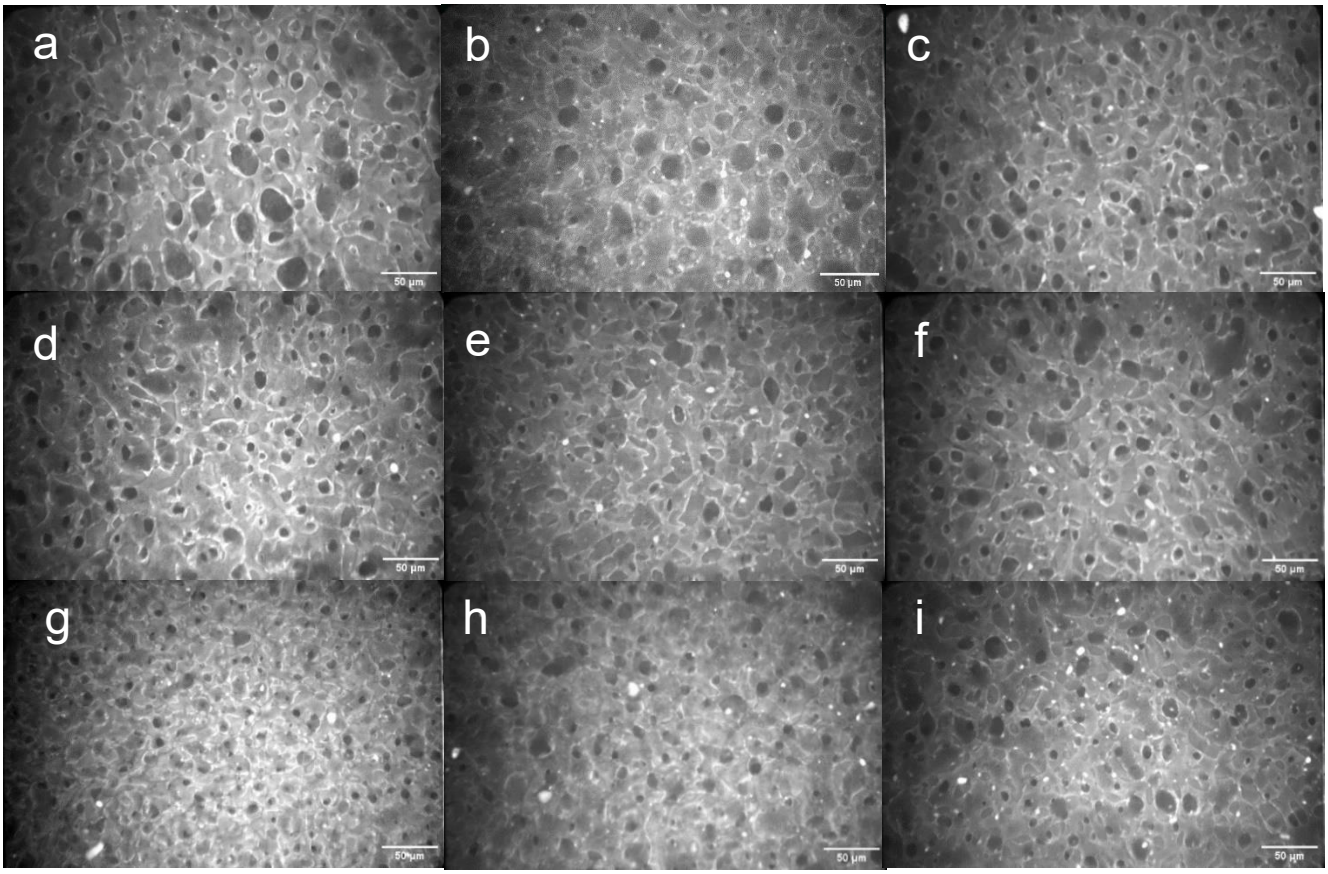

Figure 22: 2CMETS bijels checked 8 days after synthesis.

a) $\phi_{2CMETS} = 9.07 \text{ x } 10^{-3}$ b) $\phi_{2CMETS} = 9.82 \text{ x } 10^{-3}$ c) $\phi_{2CMETS} = 10.6 \text{ x } 10^{-3}$

d) $\phi_{2CMETS} = 11.3 \text{ x } 10^{-3}$ e) $\phi_{2CMETS} = 12.1 \text{ x } 10^{-3}$ f) $\phi_{2CMETS} = 12.8 \text{ x } 10^{-3}$

g) $\phi_{2CMETS} = 13.5 \text{ x } 10^{-3}$ h) $\phi_{2CMETS} = 14.3 \text{ x } 10^{-3}$ i) $\phi_{2CMETS} = 15.0 \text{ x } 10^{-3}$

Scale bar = 50 μm

The last candidate chosen to functionalize the surface of silica was 3-(trimethoxysilyl)propyl methacrylate (TMSPM). This silanizing agent is composed of acrylate groups as end chains, similar to those found in DSDA. These acrylate groups possess the capability to bind to both themselves and DSDA during the polymerization process, effectively securing them in place along the fluid interface and keeping

structural integrity. Synthesis was identical to that of the HMDS and 2CMETS functionalized nanoparticles. However, volume fractions of TMSPM (ϕ_{TMSPM}) ranging from 19.4 x 10^{-3} to 31.0 x 10^{-3} were added evenly across nine vials. Following synthesis, particles were washed in a similar manner and allowed to dry before having their wettability checked via bijel imaging. An illustration of silicas decorated surface is represented, as well as the particles' average size distribution (Figures 23 & 24). All nine batches were tested using the same protocol, and their wettability was examined based on the evenness of the bijel structure (Figure 25). As time progressed and the particles were stored in a dark environment, the surface chemistry shifted towards neutrally wetting. Therefore, bijels were observed to have a more even structure (Figure 26).

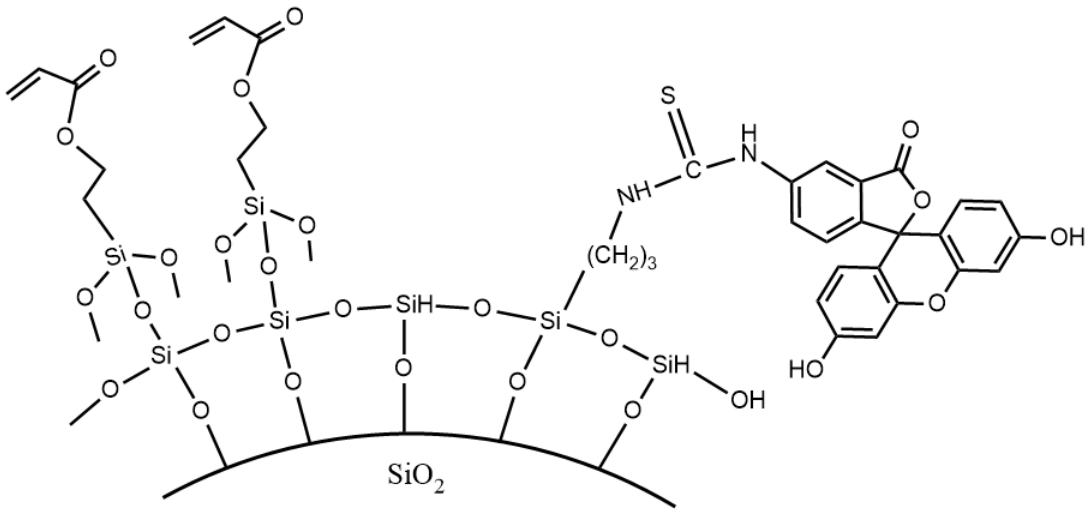

Figure 23: Surface chemistry of silica nanoparticles with TMSPM and FITC/APTES dye complex

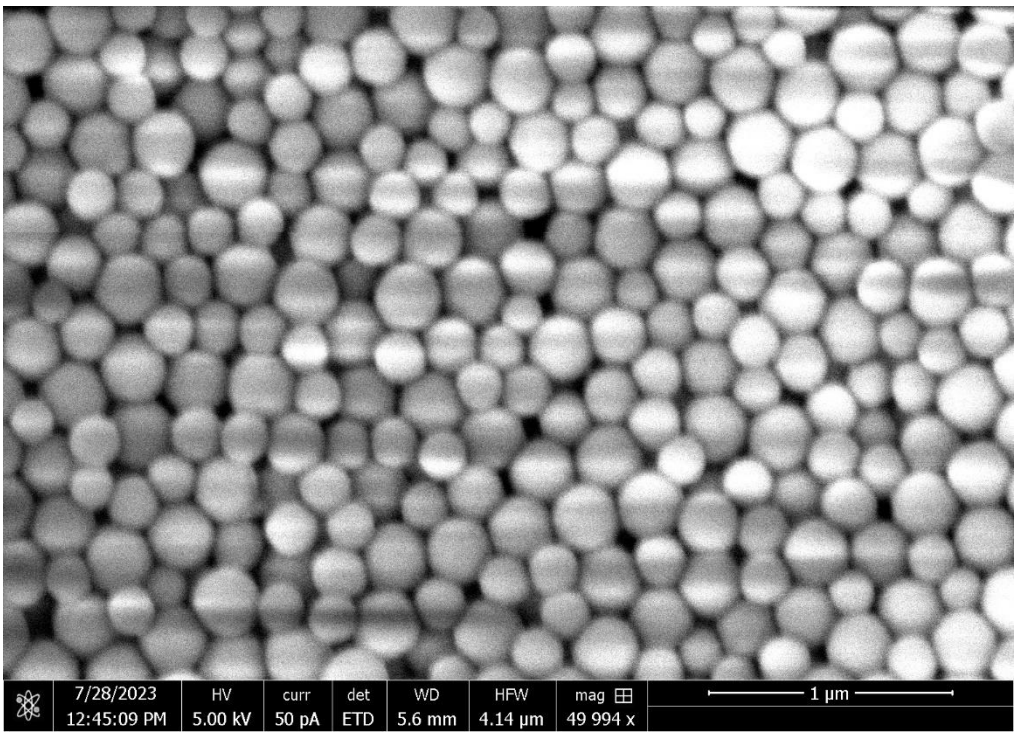

Figure 24: SEM of TMSPM silica nanoparticles with an average diameter ~ 214 nm

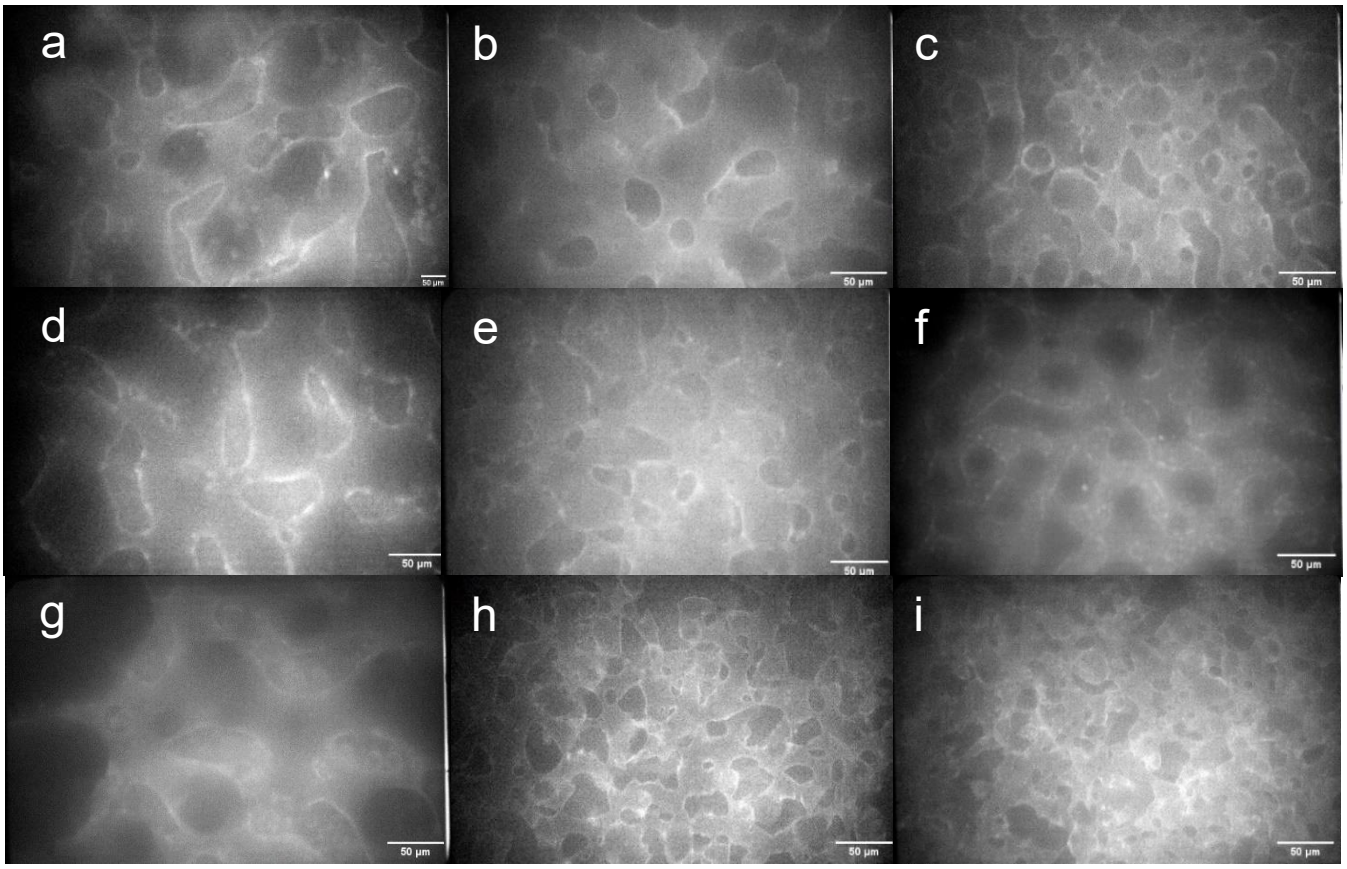

Figure 25: TMSPM bijels checked immediately upon synthesis.

a) $\phi_{TMSPM} = 19.4 \text{ x } 10^{-3}$ b) $\phi_{TMSPM} = 20.9 \text{ x } 10^{-3}$ c) $\phi_{TMSPM} = 22.4 \text{ x } 10^{-3}$

d) $\phi_{TMSPM} = 23.8 \text{ x } 10^{-3}$ e) $\phi_{TMSPM} = 25.3 \text{ x } 10^{-3}$ f) $\phi_{TMSPM} = 26.7 \text{ x } 10^{-3}$

g) $\phi_{TMSPM} = 28.2 \text{ x } 10^{-3}$ h) $\phi_{TMSPM} = 29.6 \text{ x } 10^{-3}$ i) $\phi_{TMSPM} = 31.0 \text{ x } 10^{-3}$

Scale bar = 50 μm

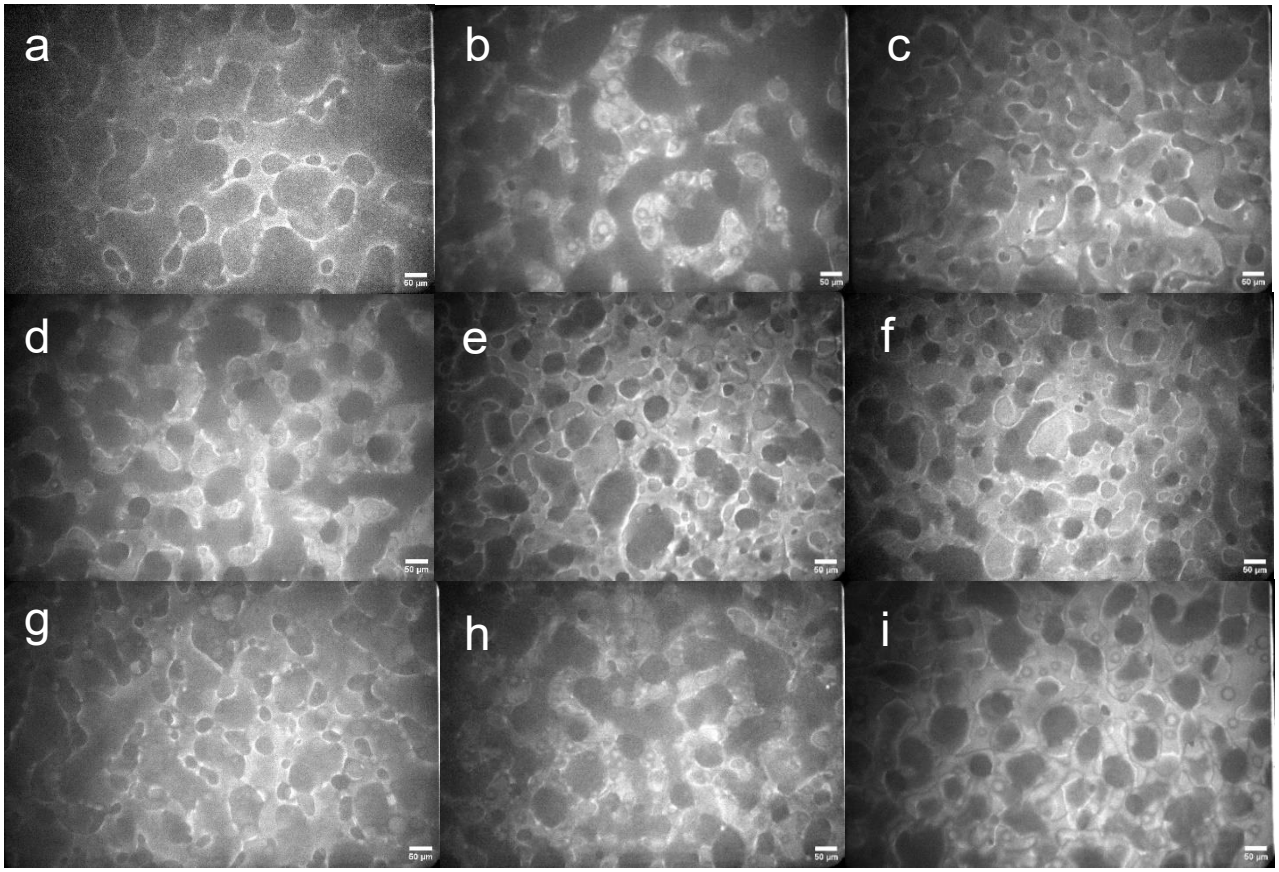

Figure 26: TMSPM bijels checked 2 months after synthesis.

a) $\phi_{TMSPM} = 19.4 \text{ x } 10^{-3}$ b) $\phi_{TMSPM} = 20.9 \text{ x } 10^{-3}$ c) $\phi_{TMSPM} = 22.4 \text{ x } 10^{-3}$

d) $\phi_{TMSPM} = 23.8 \text{ x } 10^{-3}$ e) $\phi_{TMSPM} = 25.3 \text{ x } 10^{-3}$ f) $\phi_{TMSPM} = 26.7 \text{ x } 10^{-3}$

g) $\phi_{TMSPM} = 28.2 \text{ x } 10^{-3}$ h) $\phi_{TMSPM} = 29.6 \text{ x } 10^{-3}$ i) $\phi_{TMSPM} = 31.0 \text{ x } 10^{-3}$

Scale bar = 50 μm

2.2 Summary

Expanding upon the methods initially introduced by Ching and Mohraz in 2021, we successfully synthesized DSDA, a PEGDA-like monomer containing a disulfide bond with high yields and scalability. Extensive research was conducted to identify an alcohol exhibiting partial miscibility with DSDA, leading to the selection of 1,2-pentanediol as the

most suitable candidate. Experimental techniques, such as cloud point and turbidity analysis, were used to create a phase diagram that results in an UCST of 14.28 °C at a critical mass fraction of 54% DSDA to 46% 1,2-PD. Analysis of silanizing agents like 2CMETS and TMSPM enabled bijel formation with controllable wetting properties. Moreover, the surface chemistry of these particles shifted over time to become neutrally wetting, eliminating the need for extensive oven tuning. Overall, this breakthrough introduces a new degradable bijel system, expanding the available options in our material library.

Chapter 3. Polymerization & Degradation of Bijel Templated Materials

3.1 Introduction

IPBs present a robust and distinctive approach to template a bicontinuous fluid-fluid system into an interpenetrating porous material. A bijel system was created using a disulfide-based monomer, which, upon polymerization into a solid scaffold, allows a reducing agent to cleave these bonds, facilitating degradation. Scientific literature has explored the use of 1,4-dithiothreitol (DTT) as a reducing agent that effectively cleaves disulfide bonds.[46–49] Through extensive research, both polymerization and quenching methods were optimized to create a porous scaffold comprised of our DSDA/1,2-PD system. Therefore, a novel concept called a bijel templated invertible mold (BTIM) is introduced. The process involves filling the void space with a desired polymerizable complex and, subsequently, degrading the solid DSDA phase, resulting in an inverted scaffold composed of the chosen material of interest. This process will increase the utility of spinodal architectures and allow new materials to possess bijel's unique microstructure.

3.2 Materials

The following chemicals were used as received. Hydroquinone (≥ 99%), 1,4-Dithiothreitol, and Irgacure 2959 were purchased from Sigma-Aldrich. 2,2-Dimethoxy-2-phenylacetophenone (DMPA) (99%) was purchased from Thermo Fisher Scientific.

3.3 Polymerization of APTES & 2CMETS Bijels

Initial investigations of polymerization began using the first set of neutrally wetting particles that enabled bijel formation, APTES functionalized nanoparticles. To create BTMs, glass cylindrical tubes adhered to glass slides were used as molds. These tubes were filled with a bijel mixture at critical composition, consisting of a DSDA solution with 1% Irgacure 2959 by mass, a 1 mM solution of 1,2-PD with sodium fluorescein salt, and 2.5 mg APTES functionalized nanoparticles. Samples were then quenched in a -40 °C cold bath for 10 minutes, covered with an integrating sphere, and flashed with UV (OmniCure, series 2000, 200 W, 325-385 nm) at 80% power for 1 minute. This resulted in the outer walls of the BTM polymerizing into a structured solid while the inner region of the cylinder remained in a liquid state (Figure 27). To try a different approach, 2CMETS functionalized nanoparticles were mixed, quenched, and polymerized in DSDA and 1,2-PD using the same method. The same type of result was observed where now the whole sample would be a soft, white, polymerized monomer and alcohol mixture. We hypothesized this was a result of photoinhibition, where the functionalized nanoparticles with amine groups acts as a hindered amine stabilizer further quenching photons from reaching the center.[51] Likewise, ester groups act as photosensitive dissolution inhibitors for acrylate containing polymers.[52]

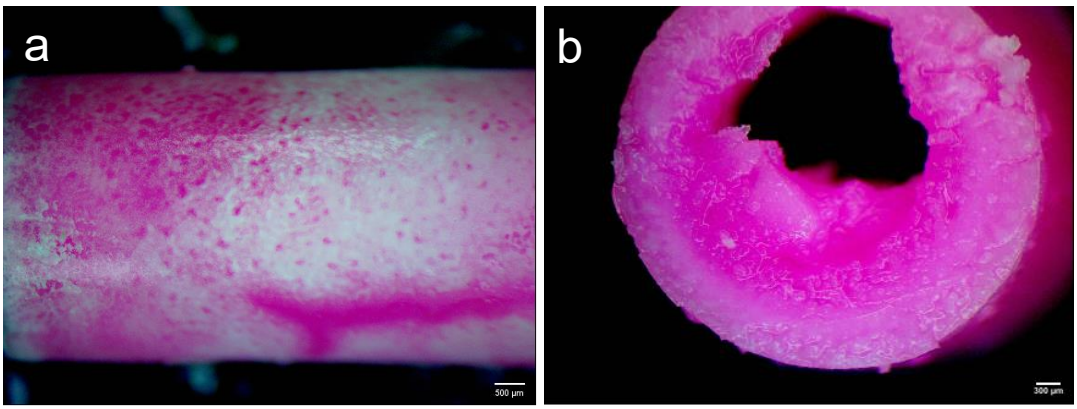

Figure 27: Polymerization of bijel with APTES nanoparticles and Irgacure 2959 leading to an unpolymerized center. Scale bar = 500 μm (a) & 300 μm (b)

3.4 Polymerization Characterization

For the investigation of phase separation and the quenching impact of sodium fluorescein salt within the monomer-poor phase, we generated two fluid batches. Each batch contained a 1% Irgacure solution by mass, where one batch also included 0.1 mM of sodium fluorescein salt in 1,2-PD, while the other contained plain 1,2-PD. The objective was to allow these fluids to phase separate in a 0 °C environment overnight, pipette the top layer (1,2-PD) and pipette the bottom layer (DSDA) and subject them both to UV to test if one phase polymerizes while the other does not. Our initial hypotheses suggested that the monomer-poor phase, consisting of primarily 1,2-PD with a small amount of DSDA, would still polymerize due to the low amount of monomer and photoinitiator present. However, the main purpose was to see if the quencher would absorb all the photons required to prevent the monomer-poor phase from polymerizing. UV light was irradiated at 25% power for 5 minutes, resulting in both the top layer and bottom layer polymerizing with different textures of solidification (Figure 28). With both

the presence and absence of sodium fluorescein salt (Figure 29), the top layer (monomer-poor phase) consisted of a white gooey solid while the bottom layer (monomer-rich phase) polymerized into a solid clear cylinder. Therefore, this evidence shows that it was the remaining DSDA in the alcohol phase that was preventing photons from penetrating the sample, as well as causing a shell to form.

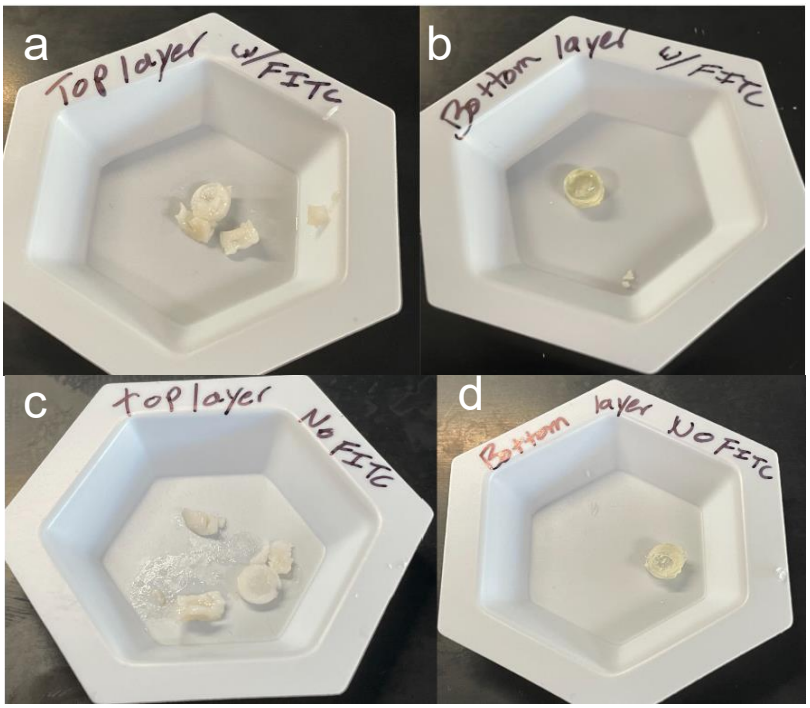

Figure 28: Polymerization of top layer and bottom layer post phase separation. a) 1,2-PD (top) layer with no sodium fluorescein salt (labeled FITC here) b) DSDA (bottom) layer with no FITC c) 1,2-PD layer with FITC d) DSDA layer with FITC

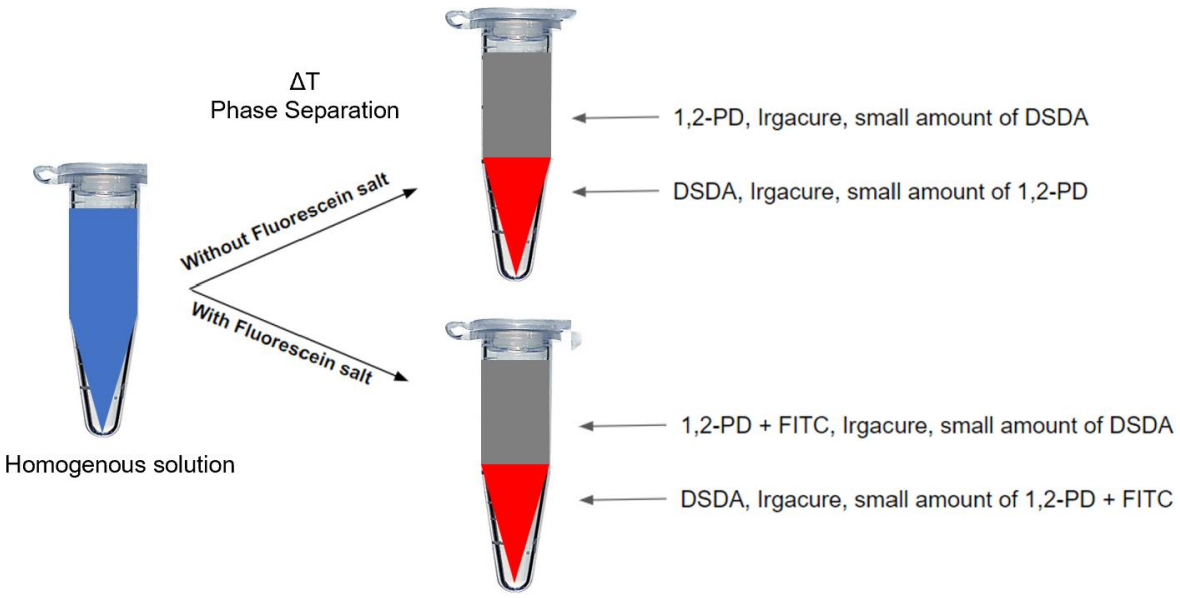

Figure 29: Phase separation schematic with labeled components

To identify a photoinitiator that selectively favors DSDA over 1,2-PD, we conducted a screening process over a range of photoinitiators in our lab, ultimately choosing 2,2-dimethoxy-2-phenylacetophenone (DMPA) as a suitable candidate. However, concerns arose about UV light penetration into the monomer-rich region (DSDA and 1,2-PD) through the monomer-poor region (1,2-PD and DSDA), as depicted in Figure 27, which shows an unpolymerized center. To test polymerization, we prepared a fluid sample using a 1% by mass solution of DMPA in DSDA, allowing phase separation in a 0 °C environment overnight. Two concentric cylinders were stacked, with the monomer-poor region placed in the upper cylindrical mold and the monomer-rich region placed in the lower mold, to investigate the polymerization process (Figure 30). The lower cylindrical mold was covered with aluminum foil to prevent UV light (20% power, 1 min) from penetrating the sides and to enable exposure solely through the top, ensuring that UV radiation passed through the monomer-poor phase before reaching the monomer-rich phase. Initially we hypothesized that UV light would pass through,

resulting in the same soft, white, monomer-poor phase and a clear, solidified, monomer-rich phase. This was confirmed by extracting the samples from their molds, revealing that 1,2-PD does allow UV light to penetrate and polymerize the monomer-rich, DSDA phase.

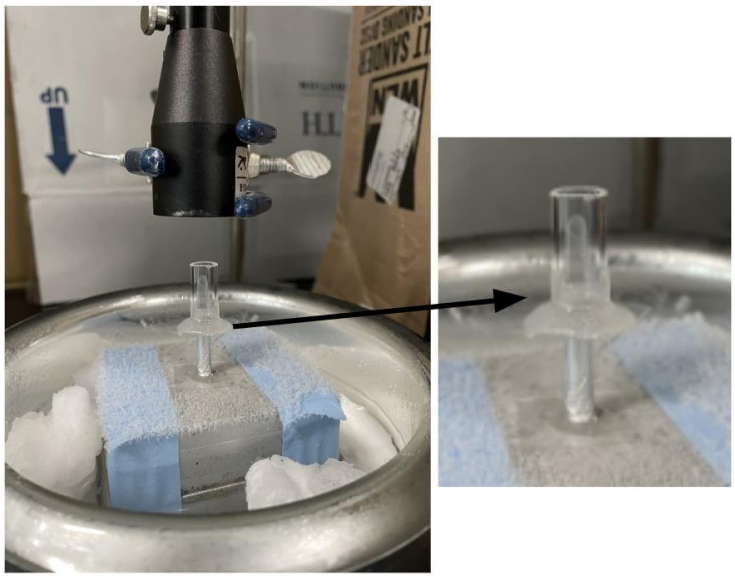

Figure 30: Polymerization via concentric tubes. UV passing through the monomer-poor region (top tube) to polymerize the monomer-rich region (bottom tube)

3.5 Polymerization of BTM Sheets

Synthesizing nanoparticles with surface functionalization consisting of TMSPM offered polymerization of the bulk volume rather than lack of polymerization in certain areas. Incorporating methacrylate groups onto the particles surface that can split and form new bonds in the presence of UV was the solution leading to form BTM sheets of comprised of DSDA. An illustration showing the particle-DSDA interaction upon polymerization shows a new bond being formed at the fluid interface (Figure 31). Chain growth is propagated by homolytically cleaving a π bond, where one electron forms a σ

bond with the attacking reagent on one alkene carbon, while the other electron remains attached to the first alkene carbon. This mechanism of radial chain polymerization proceeds, forming new π bonds until termination is reached.

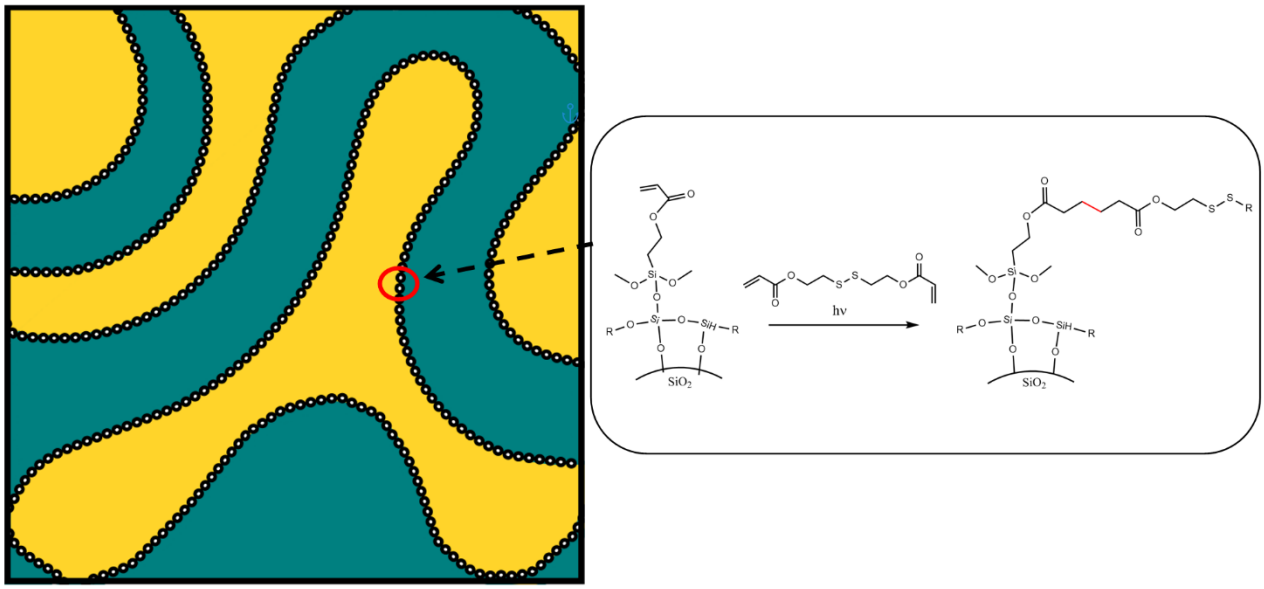

Figure 31: Particle-DSDA interaction reaction under the presence of UV. Blue phase represents DSDA while yellow phase represents 1,2-PD. Red bond indicates new bond formed.

While polymerization throughout the volume was achieved, the pendulum swung in the opposite direction, solidifying both phases of the BTM. Results demonstrated via Ching and Mohraz, 2021, implied that the use of a hydrophilic fluorescent dye such as sodium fluorescein salt in the presence of DMPA, a hydrophobic photoinitiator, at ratios of 0.1 mM and 1 mM, respectively, would quench photons in the monomer-poor region. This, however, was not the case in the DSDA/1,2-PD system as both phases consistently polymerized upon exposure to UV at 20% power for 30 seconds (Figure 32).

To create these DSDA BTM sheets, a 22.5 mm x 11.5 mm rectangular mold (inner area) was created out of PDMS 184 adhered onto a 24 x 60 mm coverslip (VWR Avantor) using PDMS 184 as an adhering agent. A bijel mixture was then made in a 1.5 mL centrifuge tube using 2 mg of neutrally wetting TMSPM functionalized nanoparticles, suspending them in 128 mg of a 1 mM DSDA solution containing 2,2-dimethoxy-2-phenylacetophenone (DMPA) as a photoinitiator. The suspension was mixed using an ultrasonic horn (Branson Sonifier 250) for 30 seconds at 4 W. After subjecting the mixture to sonication. The sample was reweighed on a scale to determine the mass of DSDA, allowing for the calculation of the corresponding amount of 1,2-pentanediol required to achieve a critical mass fraction of 54% DSDA and 46% 1,2-pentanediol. Before being added to the bijel suspension, a homogeneous mixture of sodium fluorescein salt with a concentration of 1 mM was prepared and combined with 1,2-pentanediol, serving as a fluorescent dye essential for quenching photons in the monomer-poor phase following phase separation. The sample was subjected to further sonication using an ultrasonic horn at 4 W for 20 seconds, followed by immersion in a sonicating bath (Branson 1510) for 5 minutes to achieve a homogeneous solution with a total volume of 200-220 µL. Next, the sample was vortexed and 145 µL was added to the PDMS/glass mold stored in a 75 °C oven and left to incubate for 30 seconds before being quickly quenched by placing it on an aluminum cold block immersed in a -40 °C bath containing dry ice and acetonitrile. The bijel sample passed through its transition temperature, indicated by a color change from yellow to dark white, and was allowed to remain quenched at -40 °C for 10 minutes. A UV lamp containing a 325-385 nm bandpass filter was used to irradiate the sample at 20% power for 1 minute, initiating

polymerization. The sample was then washed thoroughly with isopropanol and subsequently dried in a 100 °C oven for 15 minutes before checking the sample's microstructure on a stereoscope and left in a 75 °C oven overnight.

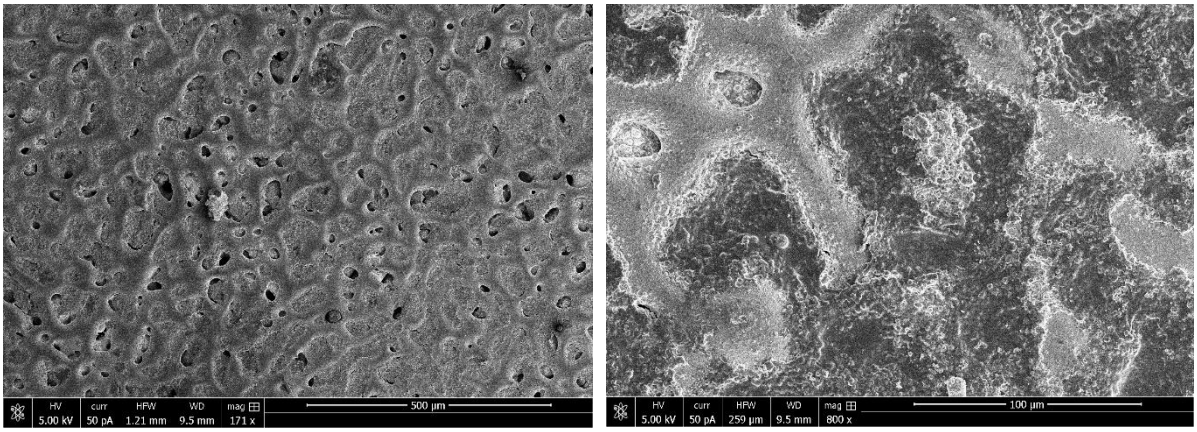

Figure 32: SEM Image of both phases polymerized upon exposure to UV light in the presence of 1 mM sodium fluorescein salt (dye) as a quencher.

To address this polymerization concern, higher concentrations of dye were tested to see which concentration would quench photons in the monomer-poor region. Various concentrations of sodium fluorescein salt in 1,2-PD were tested with molarity values ranging from 1 mM to 10.6 mM using the same protocol previously mentioned. Dye concentrations greater than 10.6 mM led to no polymerization whereas concentration below 8 mM led to both phases polymerizing. However, between 8-10 mM, some areas that were desired to be void spaces were still polymerized. To solve this issue a free radical scavenger was incorporated into the bijel mixture to act as a photon quencher in the monomer-poor phase. Free radical scavengers have been utilized in producing therapeutic drugs, supplements, and food additives as powerful antioxidants.[53] For this reason, hydroquinone (HQ), a two-hydroxy phenol with alcohol groups situated at the para positions of a benzene ring, was chosen for this purpose. Incorporating HQ into the

bijel mixture involved assessing its miscibility with DSDA and 1,2-PD. As such, HQ was found to be miscible with 1,2-PD and immiscible with DSDA. This suggested that the addition of a free radical scavenger would preferentially favor the 1,2-PD monomer-poor phase rather than the DSDA monomer-rich phase. Thus, using the same BTM method as previous, now with a sodium fluorescein salt concentration of 2.66 mM in 1,2-pentanediol, 3 mg of HQ (263 mM in 1,2-PD) was added to the overall mixture such that the total sample volume ranged from 200-220 µL. A proper balance of dye to free radical scavenger allowed for successful photons quenching in the monomer-poor phase. BTM sheets were created with repeatability consisting of two-three repeat units of bicontinuous structure shown via Scanning Electron Miscopy (SEM) images (Figure 33).

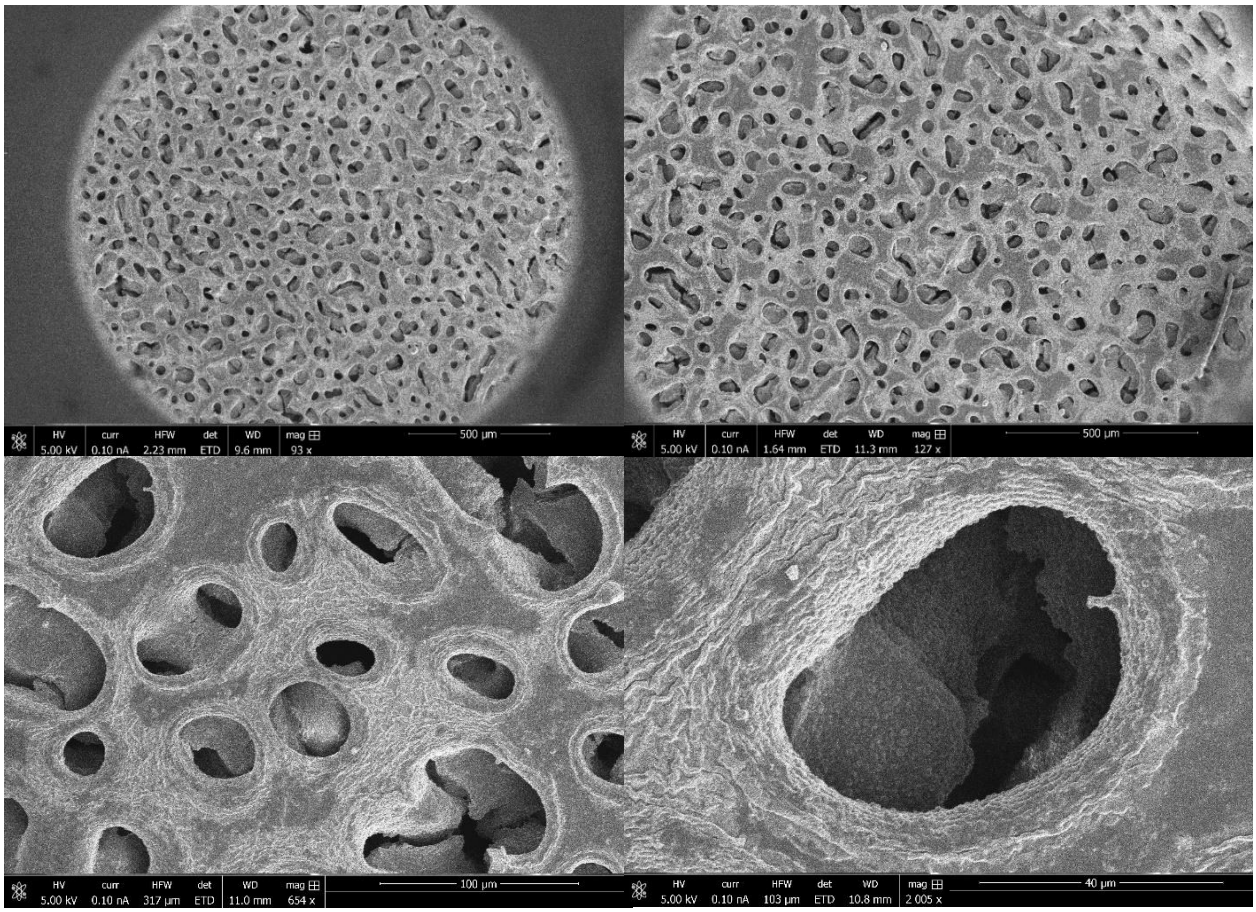

Figure 33: SEM images of DSDA BTM sheet

To further demonstrate quenching photons in the monomer-poor region, samples were created with and without additives to show that sodium fluorescein salt and hydroquinone indeed act as quenchers in parallel. Four samples with fluids were prepared, each with a critical composition of 54% DSDA with various additives. The first sample had a 1 mM DMPA in DSDA solution. The second 1 mM DMPA in DSDA and 2.66 mM sodium fluorescein salt in 1,2-PD. The third, 1 mM DMPA in DSDA and 263 mM HQ in 1,2-PD, while the fourth had 1 mM DMPA in DSDA, 2.66 mM sodium fluorescein salt in 1,2-PD, and 263 mM HQ in 1,2-PD (Table 1). The mixtures were mixed via an ultrasonic horn (Branson Sonifier 250) and allowed to phase separate at 0 °C. The top layer (1,2-PD) and bottom layer (DSDA) were then extracted and transferred into their own rectangular PDMS mold. UV light was applied at 20% power for 1 minute to each layer to assess polymerization. In the first 3 experiments, each containing only sodium fluorescein or only hydroquinone, resulted in a polymerized solid mass. However, the experiment containing both sodium fluorescein and hydroquinone did not polymerize, resulting in a liquid phase, demonstrating the effect of local photon quenching (Figure 34).

	Photoinitiator (DMPA 1 mM)	Sodium Fluorecein Salt (2.66 mM)	Hydroquinone (263 mM)	Monomer-Poor phase polymerized? (Yes or No)
Experiment 1	✓			Yes
Experiment 2	✓	✓		Yes
Experiment 3	✓		✓	Yes
Experiment 4	✓	✓	✓	No

Table 1: Samples indicating contaning additives and polymerization results

Figure 34: Samples post UV irradiation. Experiment 1-3 showed polymerization of the top layer indicated by rectangular sheets, whereas experiment 4 showed an unpolymerized top layer, shown via liquid spreading on glass.

3.6 Degradation of BTM Sheets

The purpose of the disulfide bonds is to have the ability to degrade the BTM. A BTM was divided into two halves, with one part submerged in a 300 mM DTT and 157 mM tris buffer aqueous solution in a nitrogen atmosphere to maintain a pH ranging from approximately 8.6-8.8. The second half was placed in an identical solution minus the DTT. To maintain an airtight environment, the vial was sealed with a rubber septum and parafilm, then covered with foil and parafilm again. Vacuum was applied to the vial using a Schlenk line connected to a rotary vane vacuum pump, reaching a pressure between 1×10^{-2} and 1×10^{-4} mbar. All the oxygen in the sample was replaced with nitrogen over a 5-minute period. Each sample was sonicated (Branson 1510) for 3 days, with the

solutions replaced halfway through the experiment. After 72 hours, the first half that was subjected to the reducing agent had dissolved, whereas the control stayed completely intact (Figure 35). Losing only 11.03% of the initial mass, we believe this was due to the constant force exerted by sonification (Table 2).

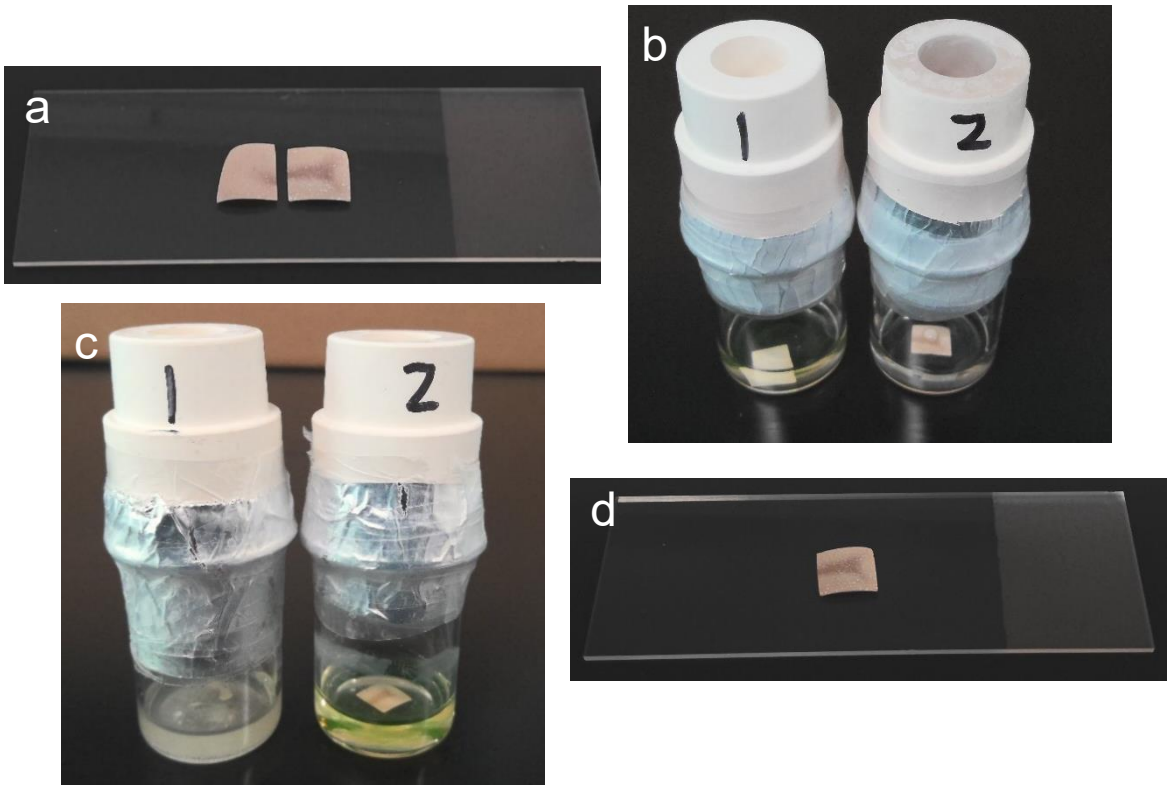

Figure 35: a) BTM cut in half, left slice (slice 1) placed in 300 mM DTT solution, right slice (slice 2) placed in water solution. b) Samples wrapped with parafilm and foil prior to sonication. c) Samples the following morning post sonication.

d) Slice 2 post sonication.

	Mass before Sonication (mg)	Mass after sonication (mg)	Mass Change (%)
Slice 1 (300 mM DTT)	12.91		Degraded Fully
Slice 2 (H_2O)	13.13	11.86	11.03

Table 2: Mass change of BTM before and after sonication with DTT

3.7 Summary

The nature of polymerizing IPB systems inherently causes both phases to polymerize in the absence of a photon quencher. We attempted the successful method used in previous IPB systems with 1,4-butanediol and PEGDA 250, which involved a 0.1 mM solution of sodium fluorescein salt, but unfortunately, it did not work with our DSDA/1,2-pentanediol system. We also observed photoinhibition when nanoparticles functionalized with amine and ester groups were used to form BTMs. These problems were solved using TMSPM, a silanizing agent with methacrylate based functional groups. However, using this method led to the polymerization of both phases. To achieve a scaffold with porous domains, we used hydroquinone, a free radical scavenger, in combination with higher concentrations of sodium fluorescein salt. After incorporating and optimizing the two components into the DSDA and 1,2-PD mixture, along with a selectively partitioning photoinitiator, the monomer-poor phase remained unpolymerized. As a result, we carried out the degradation of the BTM over a span of 3 days to achieve the desired outcome. The main objective of this research is to introduce an additional polymerizable component into the void phase, degrade the DSDA phase, and ultimately obtain a BTIM composed of the desired material. Hence, the conducted

experiments offer compelling proof regarding the degradability of these DSDA sheets, thereby introducing a novel BTM scaffold into the repertoire of already established materials known for their degradable characteristics.

Chapter 4: Future Work & Conclusion

4.1 Future Work

The extensive research conducted in this thesis has contributed to developing a novel IPB system with a key emphasis on its degradability. Consequently, this degradable sheet holds the potential to serve as a template for the creation of a BTIM using any desired polymerizable material. Despite the limitations imposed by geometric constraints arising from the limitations of mass transfer during phase separation, the production of bicontinuous and porous sheets has proven to be a successful outcome. Therefore, future work will consist of creating porous coatings where applications can be utilized in areas of tissue engineering, electrolysis, and fuel cell devices.

Subsequent efforts to significantly broaden the chemical library of degradable BTMs could involve emphasizing the development of a larger polymer featuring multiple disulfide bonds, accompanied by acrylate groups as terminal chains. Extending the carbon chain's length or incorporating additional chains with multiple disulfide bonds, as opposed to just one as seen in DSDA, might change the degradation rates of solid scaffolds. Upon successful synthesis or acquisition of this polymer, the entire process of constructing a bijel from the ground up, similar to the methodology detailed in this paper, would need to be executed. For regulating degradation rates over time, it's worth exploring the effects of increased concentrations of DTT under inert conditions. Higher

concentrations are likely to yield more rapid degradation outcomes compared to lower concentrations. It's important to note that degradation treatments could influence the mechanical properties of BTMs, potentially leading to a reduction in structural integrity.

Implantable materials and prosthetics subjected to drug delivery and tissue integration are carefully designed to interact effectively with the human body. To mitigate the foreign body response associated with these materials, the integration of a BTM coating has emerged as a promising approach. It becomes possible to reduce the adverse reactions triggered by the foreign body response by applying a porous coating onto the implant material.[9,12] A notable embodiment involves using an bijel templated invertible mold (BTIM) that can be used to template the spinodal geometry of biopolymer-based scaffolds such as collagen. This can allow cells to be seeded and implanted into the body, allowing for cellular infiltration and tissue regeneration. Using a material of bicontinuous nature enhances vascularization and contributes to an enhanced macrophage response mechanisms by increasing the available percentage of pro-healing M2 phenotypes. Not only can this be utilized for drug delivery, but implantable materials such as prosthetics can be coated with a polymeric bijel sheet to further mitigate the foreign body response improve implant performance.[54] The potential of utilizing BTIMs and constructing scaffolds from innovative materials hold great promise for future research. The unique microstructural characteristics of bijels offers innovative opportunities, with the ability to impact the field of regenerative medicine.

The renewable energy sector has placed significant emphasis on developing efficient transport layers for electrolysis and fuel cell devices, aiming to create cleaner energy solutions. One promising avenue for future work involves utilizing BTIM as

sheets to enhance material coatings, which could result in substantial improvements in mass transfer within these devices. Such advancements have the potential to increase the performance and efficiency of electrolysis and fuel cell technologies, optimizing the distribution of reactants and products to and from the catalyst layers, ultimately paving the way for sustainable and cleaner energy solutions. This type of research holds promise for driving further advancements in renewable energy technologies, bringing us closer to a greener and more environmentally friendly future.

4.2 Conclusion

Through scientific progression researchers harness thermodynamic and transport phenomena principles to create novel porous materials. In this body of work, an intrinsically polymerizable bijel system capable of degradation through a chemical trigger was successfully created. This included finding a partial miscible system with DSDA, mapping a phase diagram, synthesizing neutrally wetting colloidal particles, and solely polymerizing the monomer-rich phase to inevitably create a porous scaffold. This work hereby shows the extent to which bijels can be explored through polymers, solvents, and alcohols of various means. To expand the library of available bijels and degradable BTMs even further, an opportunity emerges in synthesizing disulfide-containing polymers with extended carbon chains featuring methacrylate end groups. However, by suggesting future work of a BTIM, the further spectrum of functional, bicontinuous, porous materials can be widened to allow more compounds to exhibit the same microstructural properties bijels offer. While the idea of creating porous coatings for surfaces in tissue engineering, electrolysers, and fuel cell devices might appear superficial, the choice of the right material can lead to innovative results with significant

implications. These exciting ideas provide researchers with a broader foundation to extend the findings showcased in this thesis, creating opportunities for the development of novel spinodal like materials and the expansion of the library of bijels and BTMs.

Appendix

A1: 100% DSDA calibration cooling sweep (70 °C to 20 °C)

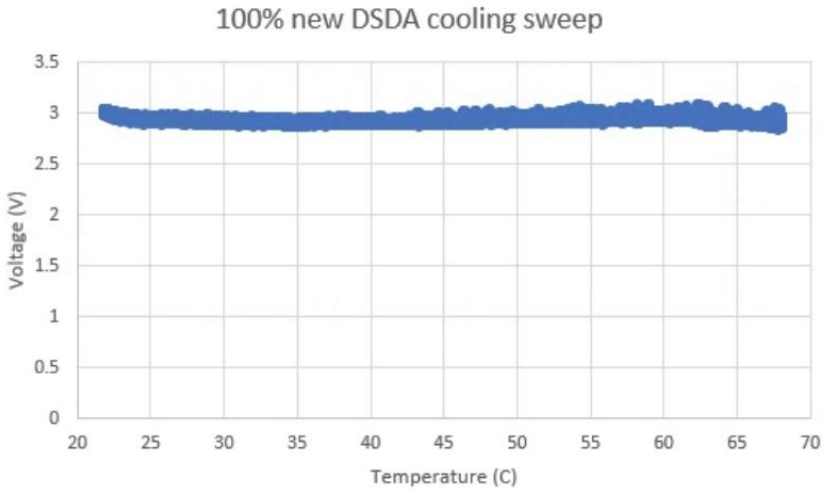

A2: Cloud point data passed through Matlab code to give intersection point of the solutions transition temperature.

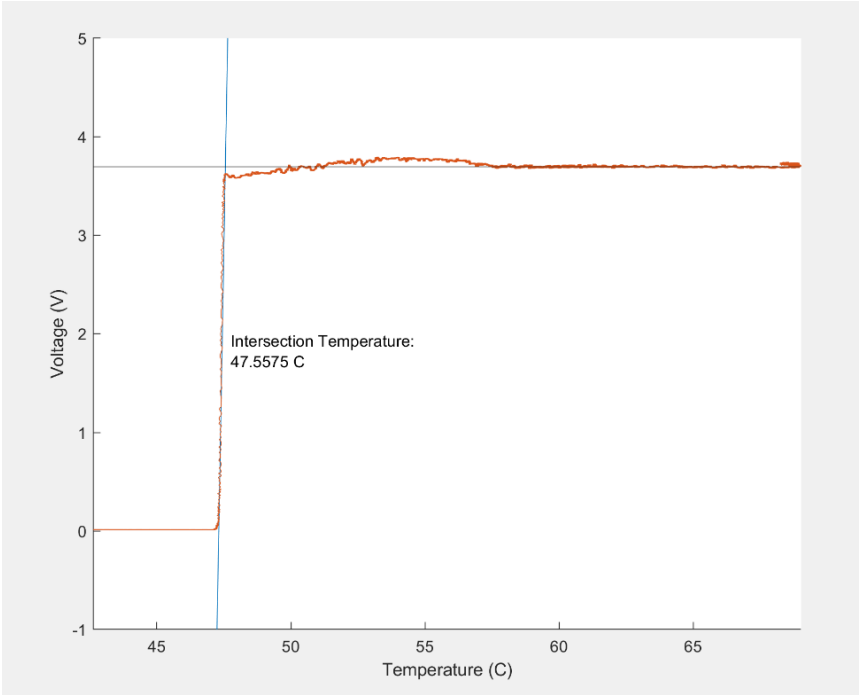

References

(1) *Hierarchical porous materials for tissue engineering*. https://doi.org/10.1098/rsta.2005.1689.
(2) Perego, C.; Millini, R. Porous Materials in Catalysis: Challenges for Mesoporous Materials. *Chem. Soc. Rev.* **2013**, *42* (9), 3956–3976. https://doi.org/10.1039/C2CS35244C.
(3) Wang, H.; Wang, X.; Li, M.; Zheng, L.; Guan, D.; Huang, X.; Xu, J.; Yu, J. Porous Materials Applied in Nonaqueous Li–O2 Batteries: Status and Perspectives. *Advanced Materials* **2020**, *32* (44), 2002559. https://doi.org/10.1002/adma.202002559.
(4) Zhou, J.; Wang, B. Emerging Crystalline Porous Materials as a Multifunctional Platform for Electrochemical Energy Storage. *Chem. Soc. Rev.* **2017**, *46* (22), 6927–6945. https://doi.org/10.1039/C7CS00283A.
(5) *Engineering porous materials for fuel cell applications*. https://doi.org/10.1098/rsta.2005.1684.
(6) Kristian Stevik, T.; Kari Aa; Ausland, G.; Fredrik Hanssen, J. Retention and Removal of Pathogenic Bacteria in Wastewater Percolating through Porous Media: A Review. *Water Research* **2004**, *38* (6), 1355–1367. https://doi.org/10.1016/j.watres.2003.12.024.
(7) Ponte, C. Design of porous materials for environmental remediation.
(8) Lutzweiler, G.; Ndreu Halili, A.; Engin Vrana, N. The Overview of Porous, Bioactive Scaffolds as Instructive Biomaterials for Tissue Regeneration and Their Clinical Translation. *Pharmaceutics* **2020**, *12* (7), 602. https://doi.org/10.3390/pharmaceutics12070602.
(9) *Bijel-templated implantable biomaterials for enhancing tissue integration and vascularization | Elsevier Enhanced Reader*. https://doi.org/10.1016/j.actbio.2019.06.031.
(10) Hady, T. F.; Hwang, B.; Pusic, A. D.; Waworuntu, R. L.; Mulligan, M.; Ratner, B.; Bryers, J. D. Uniform 40-Mm-Pore Diameter Precision Templated Scaffolds Promote a pro-Healing Host Response by Extracellular Vesicle Immune Communication. *J Tissue Eng Regen Med* **2021**, *15* (1), 24–36. https://doi.org/10.1002/term.3160.
(11) Teng, W.; Long, T. J.; Zhang, Q.; Yao, K.; Shen, T. T.; Ratner, B. D. A Tough, Precision-Porous Hydrogel Scaffold: Ophthalmologic Applications. *Biomaterials* **2014**, *35* (32), 8916–8926. https://doi.org/10.1016/j.biomaterials.2014.07.013.
(12) Thorson, T. J.; Botvinick, E. L.; Mohraz, A. Composite Bijel-Templated Hydrogels for Cell Delivery. *ACS Biomater. Sci. Eng.* **2018**, *4* (2), 587–594. https://doi.org/10.1021/acsbiomaterials.7b00809.
(13) Goyal, B.; Pandey, A. Critical Review on Porous Material Manufacturing Techniques, Properties & Their Applications. *Materials Today: Proceedings* **2021**, *46*, 8196–8203. https://doi.org/10.1016/j.matpr.2021.03.163.
(14) Al-Maharma, A. Y.; Patil, S. P.; Markert, B. Effects of Porosity on the Mechanical Properties of Additively Manufactured Components: A Critical Review. *Mater. Res. Express* **2020**, *7* (12), 122001. https://doi.org/10.1088/2053-1591/abcc5d.

(15) Bruneau, C.-H.; Mortazavi, I. Numerical Modelling and Passive Flow Control Using Porous Media. *Computers & Fluids* **2008**, *37* (5), 488–498. https://doi.org/10.1016/j.compfluid.2007.07.001.
(16) *The permeability of porous materials*. https://doi.org/10.1098/rspa.1950.0068.
(17) Ching, H.; J. Thorson, T.; Paul, B.; Mohraz, A. Rapid Production of Bicontinuous Macroporous Materials Using Intrinsically Polymerizable Bijels. *Materials Advances* **2021**, *2* (15), 5067–5075.
(18) Day, G. S.; Drake, H. F.; Zhou, H.-C.; Ryder, M. R. Evolution of Porous Materials from Ancient Remedies to Modern Frameworks. *Commun Chem* **2021**, *4* (1), 114. https://doi.org/10.1038/s42004-021-00549-4.
(19) *Microstructural characteristics of bijel-templated porous materials - ScienceDirect*. https://www.sciencedirect.com/science/article/abs/pii/S2589152919301899?via%3Dihub (accessed 2023-06-24).
(20) *Forces Controlling the Assembly of Particles at Fluid Interfaces*. https://doi.org/10.1021/acs.langmuir.2c02038.
(21) Thomas, R. K.; Penfold, J. Neutron and X-Ray Reflectometry of Interfacial Systems in Colloid and Polymer Chemistry. *Current Opinion in Colloid & Interface Science* **1996**, *1* (1), 23–33. https://doi.org/10.1016/S1359-0294(96)80040-9.
(22) Lee, M. N.; Thijssen, J. H. J.; Witt, J. A.; Clegg, P. S.; Mohraz, A. Making a Robust Interfacial Scaffold: Bijel Rheology and Its Link to Processability. *Advanced Functional Materials* **2013**, *23* (4), 417–423. https://doi.org/10.1002/adfm.201201090.
(23) Pickrahn, K.; Rajaram, B.; Mohraz, A. Relationship between Microstructure, Dynamics, and Rheology in Polymer-Bridging Colloidal Gels. *Langmuir* **2010**, *26* (4), 2392–2400. https://doi.org/10.1021/la902857c.
(24) *Colloidal Jamming at Interfaces: A Route to Fluid-Bicontinuous Gels*. https://doi.org/10.1126/science.1116589.
(25) Clegg, P. S. Introduction to Bijels. 33.
(26) Herzig, E. M.; White, K. A.; Schofield, A. B.; Poon, W. C. K.; Clegg, P. S. Bicontinuous Emulsions Stabilized Solely by Colloidal Particles. *Nature Mater* **2007**, *6* (12), 966–971. https://doi.org/10.1038/nmat2055.
(27) Lee, M. N.; Mohraz, A. Bicontinuous Macroporous Materials from Bijel Templates. *Advanced Materials* **2010**, *22* (43), 4836–4841. https://doi.org/10.1002/adma.201001696.
(28) Witt, J. A.; Mumm, D. R.; Mohraz, A. Microstructural Tunability of Co-Continuous Bijel-Derived Electrodes to Provide High Energy and Power Densities. *J. Mater. Chem. A* **2016**, *4* (3), 1000–1007. https://doi.org/10.1039/C5TA06260H.
(29) Haase, M. F.; Jeon, H.; Hough, N.; Kim, J. H.; Stebe, K. J.; Lee, D. Multifunctional Nanocomposite Hollow Fiber Membranes by Solvent Transfer Induced Phase Separation. *Nat Commun* **2017**, *8* (1), 1234. https://doi.org/10.1038/s41467-017-01409-3.
(30) Di Vitantonio, G.; Wang, T.; Haase, M. F.; Stebe, K. J.; Lee, D. Robust Bijels for Reactive Separation via Silica-Reinforced Nanoparticle Layers. *ACS Nano* **2019**, *13* (1), 26–31. https://doi.org/10.1021/acsnano.8b05718.
(31) Cai, D.; Richter, F. H.; Thijssen, J. H. J.; Bruce, P. G.; Clegg, P. S. Direct Transformation of Bijels into Bicontinuous Composite Electrolytes Using a Pre-Mix

Containing Lithium Salt. *Mater. Horiz.* **2018**, *5* (3), 499–505. https://doi.org/10.1039/C7MH01038A.
(32) Haase, M. F.; Stebe, K. J.; Lee, D. Continuous Fabrication of Hierarchical and Asymmetric Bijel Microparticles, Fibers, and Membranes by Solvent Transfer-Induced Phase Separation (STRIPS). *Advanced Materials* **2015**, *27* (44), 7065–7071. https://doi.org/10.1002/adma.201503509.
(33) Thorson, T. J. Morphologically Distinct Cell Delivery Composites and Tissue Integrating Implants Processed Using Bijels, UC Irvine, 2019. https://escholarship.org/uc/item/4wq0j2kr (accessed 2023-08-27).
(34) Phase-Transformations-in-Metals-and-Alloys.Pdf. https://gateformme.files.wordpress.com/2017/04/phase-transformations-in-metals-and-alloys.pdf (accessed 2023-07-03).
(35) Mohraz, A. Post-Processing Bijels for Applications. 27.
(36) Reeves, M.; Stratford, K.; J. Thijssen, J. H. Quantitative Morphological Characterization of Bicontinuous Pickering Emulsions via Interfacial Curvatures. *Soft Matter* **2016**, *12* (18), 4082–4092. https://doi.org/10.1039/C5SM03102H.
(37) Grattoni, C. A.; Dawe, R. A.; Seah, C. Y.; Gray, J. D. Lower Critical Solution Coexistence Curve and Physical Properties (Density, Viscosity, Surface Tension, and Interfacial Tension) of 2,6-Lutidine + Water. *J. Chem. Eng. Data* **1993**, *38* (4), 516–519. https://doi.org/10.1021/je00012a008.
(38) Witt, J. A.; Mumm, D. R.; Mohraz, A. Bijel Reinforcement by Droplet Bridging: A Route to Bicontinuous Materials with Large Domains. *Soft Matter* **2013**, *9* (29), 6773. https://doi.org/10.1039/c3sm00130j.
(39) Shell, M. S. *Thermodynamics and Statistical Mechanics: An Integrated Approach*. Cambridge Core. https://doi.org/10.1017/CBO9781139028875.
(40) Van Blaaderen, A.; Vrij, A. Synthesis and Characterization of Colloidal Dispersions of Fluorescent, Monodisperse Silica Spheres. *Langmuir* **1992**, *8* (12), 2921–2931. https://doi.org/10.1021/la00048a013.
(41) Dorati, R.; Colonna, C.; Tomasi, C.; Genta, I.; Modena, T.; Conti, B. Design of 3D Hybrid Composite Scaffolds: Effect of Composition on Scaffold Structure and Cell Proliferation. *Macromolecular Symposia* **2013**, *334* (1), 106–116. https://doi.org/10.1002/masy.201300108.
(42) Kamaly, N.; Yameen, B.; Wu, J.; Farokhzad, O. C. Degradable Controlled-Release Polymers and Polymeric Nanoparticles: Mechanisms of Controlling Drug Release. *Chem Rev* **2016**, *116* (4), 2602–2663. https://doi.org/10.1021/acs.chemrev.5b00346.
(43) Rydz, J.; Sikorska, W.; Kyulavska, M.; Christova, D. Polyester-Based (Bio)Degradable Polymers as Environmentally Friendly Materials for Sustainable Development. *International Journal of Molecular Sciences* **2015**, *16* (1), 564–596. https://doi.org/10.3390/ijms16010564.
(44) Willerth, S. M.; Sakiyama-Elbert, S. E. Approaches to Neural Tissue Engineering Using Scaffolds for Drug Delivery. *Advanced Drug Delivery Reviews* **2007**, *59* (4), 325–338. https://doi.org/10.1016/j.addr.2007.03.014.
(45) Chandra, G.; Pandey, A. Biodegradable Bone Implants in Orthopedic Applications: A Review. *Biocybernetics and Biomedical Engineering* **2020**, *40* (2), 596–610. https://doi.org/10.1016/j.bbe.2020.02.003.

(46) Evans, R. M.; Fraser, J. B.; Owen, L. N. 61. Dithiols. Part III. Derivatives of Polyhydric Alcohols. *J. Chem. Soc.* **1949**, 248. https://doi.org/10.1039/jr9490000248.
(47) Alliegro, M. C. Effects of Dithiothreitol on Protein Activity Unrelated to Thiol–Disulfide Exchange: For Consideration in the Analysis of Protein Function with Cleland's Reagent. *Analytical Biochemistry* **2000**, *282* (1), 102–106. https://doi.org/10.1006/abio.2000.4557.
(48) Cleland, W. W. Dithiothreitol, a New Protective Reagent for SH Groups [*]. *Biochemistry* **1964**, *3* (4), 480–482. https://doi.org/10.1021/bi00892a002.
(49) Du, X.; Kleitz, F.; Li, X.; Huang, H.; Zhang, X.; Qiao, S.-Z. Disulfide-Bridged Organosilica Frameworks: Designed, Synthesis, Redox-Triggered Biodegradation, and Nanobiomedical Applications. *Advanced Functional Materials* **2018**, *28* (26), 1707325. https://doi.org/10.1002/adfm.201707325.
(50) Zhao, T.; Zhang, H.; Newland, B.; Aied, A.; Zhou, D.; Wang, W. Significance of Branching for Transfection: Synthesis of Highly Branched Degradable Functional Poly(Dimethylaminoethyl Methacrylate) by Vinyl Oligomer Combination. *Angewandte Chemie International Edition* **2014**, *53* (24), 6095–6100. https://doi.org/10.1002/anie.201402341.
(51) Klemchuk, P. P.; Gande, M. E. Stabilization Mechanisms of Hindered Amines. *Polymer Degradation and Stability* **1988**, *22* (3), 241–274. https://doi.org/10.1016/0141-3910(88)90014-6.
(52) Romano, A.; Roppolo, I.; Rossegger, E.; Schlögl, S.; Sangermano, M. Recent Trends in Applying Ortho-Nitrobenzyl Esters for the Design of Photo-Responsive Polymer Networks. *Materials (Basel)* **2020**, *13* (12), 2777. https://doi.org/10.3390/ma13122777.
(53) Thavasi, V.; Bettens, R. P. A.; Leong, L. P. Temperature and Solvent Effects on Radical Scavenging Ability of Phenols. *J. Phys. Chem. A* **2009**, *113* (13), 3068–3077. https://doi.org/10.1021/jp806679v.
(54) *Polymer Coating 'Hooks Up' Metal Implants with Human Bones*. plasticstoday.com. https://www.plasticstoday.com/medical/polymer-coating-hooks-metal-implants-human-bones (accessed 2023-07-18).